CELL BIOLOGY

Integrated proteogenetic analysis reveals the landscape of a mitochondrial-autophagosome synapse during PARK2-dependent mitophagy

Jin-Mi Heo[1], Nathan J. Harper[1]*, Joao A. Paulo[1], Mamie Li[2], Qikai Xu[2], Margaret Coughlin[1], Stephen J. Elledge[2], J. Wade Harper[1†]

The PINK1 protein kinase activates the PARK2 ubiquitin ligase to promote mitochondrial ubiquitylation and recruitment of ubiquitin-binding mitophagy receptors typified by OPTN and TAX1BP1. Here, we combine proximity biotinylation of OPTN and TAX1BP1 with CRISPR-Cas9–based screens for mitophagic flux to develop a spatial proteogenetic map of PARK2-dependent mitophagy. Proximity labeling of OPTN allowed visualization of a "mitochondrial-autophagosome synapse" upon mitochondrial depolarization. Proximity proteomics of OPTN and TAX1BP1 revealed numerous proteins at the synapse, including both PARK2 substrates and autophagy components. Parallel mitophagic flux screens identified proteins with roles in autophagy, vesicle formation and fusion, as well as PARK2 targets, many of which were also identified via proximity proteomics. One protein identified in both approaches, HK2, promotes assembly of a high–molecular weight complex of PINK1 and phosphorylation of ubiquitin in response to mitochondrial damage. This work provides a resource for understanding the spatial and molecular landscape of PARK2-dependent mitophagy.

INTRODUCTION

Selective autophagy refers to a process by which specific proteins, complexes, or organelles are first marked with a signal for degradation and then encapsulated in an autophagosomal structure for delivery to the lysosome where degradation occurs. In the canonical pathway for selective autophagy, the ubiquitin (Ub)–like ATG8 proteins are thought to play a critical role in cargo enrichment within the growing autophagosomal membrane (*1*, *2*). ATG8 proteins are covalently linked with phosphatidylethanolamine enriched on the autophagosomal membrane through the action of an ATG7/ATG5/ATG12 conjugation cascade and use a hydrophobic pocket to bind either cargo directly or via various cargo receptor proteins. In mammals, two major ATG8 subfamilies (LC3A, LC3B, and LC3C and GABARAP, GABARAPL1, and GABARAPL2) are used, and genetic data suggest that GABARAP family members play a unique and rate-limiting role in autophagic flux for a variety of cargo (*3*–*5*).

During the past decade, our understanding of how cargo is marked for selective autophagy has been advanced by the finding that several classes of cargo undergo ubiquitylation, typically in response to cargo damage that could be deleterious to the cell if not eliminated (*2*, *6*–*8*). Analysis of mechanisms underlying the removal of damaged mitochondria or cytoplasmic bacteria has led to a model for Ub-dependent turnover via autophagy: Here, a collection of cargo receptors, typified by OPTN, CALCOCO2 (also called NDP52), TAX1BP1, and SQSTM1 (also called p62), are thought to interact with both Ub chains attached to cargo and with ATG8 proteins via a hydrophobic LC3-interacting region (LIR) on the receptor (*8*–*10*). Recently, it has been shown that these receptors can directly associate with the RB1CC1-ULK1 complex to directly promote autophagic signaling in proximity with the damaged organelle (*11*–*14*). These and related receptors differ in their expression patterns, their modes of regulation (including phosphorylation and ubiquitylation), their selectivity for various Ub chain linkage types, and their involvement in disease but are broadly thought to regulate most Ub-dependent trafficking of cargo to the autophagy machinery (*2*).

One pathway for removal of mitochondria involves the PARK2 Ub ligase (also called PARKIN) and the PINK1 protein kinase, which together are responsible for depolarization-dependent assembly of Ub chains on mitochondrial outer membrane (MOM) proteins (*8*, *15*, *16*). PINK1 is stabilized on the MOM upon depolarization (*17*, *18*) where it phosphorylates both the Ub-like domain of PARK2 on S65 to activate its Ub ligase activity and S65 in Ub linked with proteins on the MOM (*8*, *19*–*26*). Because PARK2 is a pS65-Ub binding protein, the accumulation of pS65-Ub concomitant with Ub chain assembly leads to further PARK2 retention on the MOM and further promotes the ubiquitylation of numerous MOM proteins (*24*, *27*, *28*). Various studies have demonstrated that PARK2 ubiquitylates numerous MOM proteins, in what appears to be a largely nonselective manner (*29*–*33*). MOM ubiquitylation then drives recruitment of multiple cargo receptors to mitochondria in a process facilitated by TBK1 protein kinase (*9*, *10*, *34*–*36*). TBK1 both associates with these Ub-binding cargo receptors and phosphorylates the Ub-binding UBAN domain in OPTN to increase the affinity of the UBAN domain for K63-linked Ub chains (*9*, *36*). In a second feed-forward step, binding of OPTN to Ub through its UBAN domain results in activation of the pool of TBK1 associated with OPTN (*9*).

While it is clear that mitochondrial ubiquitylation is necessary and sufficient to promote events linked to mitophagy, many underlying questions remain. Are particular PARK2 targets on the MOM used selectively for receptor recruitment or are receptors recruited to Ub chains independently of target identity? Does the architecture of the MOM play a role in receptor recruitment? Are there additional components of the pathway that are necessary for efficient capture and autophagosomal trafficking of damaged mitochondria? At what

[1]Department of Cell Biology, Harvard Medical School, Boston, MA 02115, USA. [2]Department of Genetics, Harvard Medical School, Howard Hughes Medical Institute; Division of Genetics, Brigham and Women's Hospital, Boston, MA 02115, USA.
*Present address: Tri-Institutional PhD Program in Chemical Biology, Weill Cornell Medical College, 1300 York Avenue, Box 194, New York, NY 10065, USA.
†Corresponding author. Email: wade_harper@hms.harvard.edu

steps in the pathway do individual components on the MOM function to promote PARK2 activation and/or mitophagic flux? Here, we used two complementary approaches—APEX2-driven proximity biotinylation of Ub-binding cargo receptors and screening of mitophagic flux using focused CRISPR-Cas9 libraries—to provide a regulatory and biochemical map of PARK2-driven mitophagy. Components identified through both approaches display notable overlap, suggesting concordance of pathway function genetically in the pathway and physically at the interface between the MOM and the autophagosome, which we refer to as the "mitochondrial-autophagosome synapse." Functional analysis of HK2, which was identified using both approaches, revealed a role in the formation of a ~700-kDa PINK1 complex together with the mitochondrial translocon and efficient phosphorylation of Ub chains on mitochondria in response to depolarization. HK2 is known to associate with voltage-dependent anion channel (VDAC) proteins on the MOM (*37*), and finding that HK2's catalytic activity is not required to support PINK1 complex assembly and S65-Ub phosphorylation suggests a potential scaffolding role for HK2 in this early step in the pathway. These studies provide a resource for further dissection of the biochemical and physical landscape of PARK2-dependent mitophagy.

RESULTS

Development of a facile system for spatial analysis of mitophagy regulators

Previous studies indicate that rapidly upon depolarization, OPTN is recruited from the cytosol to a subset of fragmented mitochondria after 1 hour of depolarization (*9*, *10*, *36*). The current model is that these OPTN-positive mitochondria represent the earliest mitochondria to activate the PINK1-PARK2 pathway, and OPTN becomes "kinetically trapped" on these structures. This model is consistent with the finding that overexpression of OPTN can accelerate mitophagy (*9*). Thus, we envisioned that molecules in proximity to OPTN in these early structures could provide insight into the landscape mitophagy.

To examine the proteomic landscape of mitochondria during recruitment of Ub-binding autophagy adaptors in response to PARK2 activation, we used APEX2-driven proximity biotinylation in HeLa Flip-In TRex (HFT) cells expressing a regulatable PARK2^{WT} cassette under doxycycline control (*9*). APEX2 is an engineered ascorbate peroxidase that reacts with H_2O_2 and an aromatic small-molecule substrate to create radicals that can react preferentially with aromatic residues in proteins within a radius of ~10 nm of the APEX2 domain (*38*). OPTN is primarily composed of coiled-coil domains and forms a homodimer. In a fully extended conformation, OPTN is anticipated to be ~20 nm in length (Fig. 1A). Initially, we tested whether N-terminal tagging of OPTN with APEX2-FLAG (APEX2^{F}) affected OPTN activity by reconstituting HFT-PARK2^{WT};OPTN$^{-/-}$;NDP52$^{-/-}$;TAX1BP1$^{-/-}$ cells [referred to as triple knockout (TKO)] with near-endogenous levels of APEX2^{F}-OPTN in either wild-type (WT), E50K, or D474N forms (Fig. 1B and fig. S1A). D474 is located in the C-terminal helical region referred to as the UBAN domain, and mutation to Asn abolishes Ub binding, while the E50K mutant near the TBK1 binding site binds more avidly to TBK1 than OPTN^{WT} (Fig. 1A) (*39*, *40*). Depolarization with antimycin A/oligomycin A (AO) for 1 hour in the context of either APEX2^{F}-OPTN^{WT} or the E50K mutant resulted in TBK1^{S172} phosphorylation (Fig. 1B and fig. S1B), and these cells were competent for mitophagy (fig. S1C). In contrast, APEX2^{F}-OPTN^{D474N} failed to induce TBK1 phosphorylation or mitophagy, despite PARK2-dependent ubiquitylation of mitochondrial proteins such as TOMM20 (Fig. 1B and fig. S1, B and C). These results are consistent with the Ub binding function of OPTN being required for pathway activation (*9*, *10*, *36*) and suggest that APEX2^{F}-OPTN is a useful tool for probing OPTN function in mitophagy.

APEX2-driven visualization of OPTN recruitment at a mitochondria-autophagosome "synapse" in response to depolarization

Previous studies have demonstrated that filamentous mitochondria rapidly undergo fission in response to mitochondrial depolarization and generate aggregated mitochondria, a subset of which are decorated with autophagy receptor puncta as visualized by light microscopy (*9*, *29*, *41*). As expected, APEX2^{F}-OPTN^{WT}, but not APEX2^{F}-OPTN^{D474N}, was recruited to puncta that overlapped a small subset of fragmented mitochondria at 1 hour after depolarization (Mander's coefficient for OPTN/mitochondria = 0.96 and that for mitochondria/OPTN = 0.25) (fig. S1D), similar to that seen previously with endogenous OPTN (*9*, *10*, *34*). To elucidate the nature of these puncta and to increase the resolution beyond that possible with a light microscope, we first took advantage of the ability of APEX2 to create a snapshot of its subcellular localization by electron microscopy (EM) when used in combination with diaminobenzidine (DAB) and a brief exposure to H_2O_2 (*38*). HFT-PARK2^{WT};OPTN$^{-/-}$ cells reconstituted with APEX2^{F}-OPTN at near-endogenous levels (fig. S1A) were depolarized (1 hour) before DAB/H_2O_2 treatment and analysis of thin sections by osmium-enhanced EM (see Materials and Methods). As expected, numerous cristae-positive mitochondrial structures with an average diameter of ~500 nm were observed, indicative of mitochondrial fission or fragmentation in response to depolarization (Fig. 1, C and D). We frequently observed electron-rich DAB staining in APEX2^{F}-OPTN–expressing cells as a crescent-shaped structure adjacent to the mitochondrial fragment or, in some cases, fully surrounding the MOM of fragmented mitochondria (Fig. 1, C and D). From 150 fragmented mitochondria quantified, 22% were DAB-positive, and one-third of these had crescent-shaped staining. Notably, DAB staining density on the MOM frequently appeared as a "synapse" with a double membrane structure detected by EM and with characteristics of a double membrane–containing autophagosome or phagophore. Consistent with this interpretation and with previous data (*9*, *10*), correlated light EM (CLEM) using α-TOMM20 to mark mitochondria and α-LC3 to mark autophagosomes revealed the presence of DAB signal surrounding fragmented mitochondria and correlating with the localization of α-LC3 staining (fig. S1E). The distance between the inner leaflet of the autophagosome or phagophore and the outer leaflet of DAB-positive MOM structures was ~25 to 35 nm across independent structures analyzed by EM (see Materials and Methods). These results indicate that a subset of depolarized mitochondria generate a synapse within 1 hour that is positive for OPTN and phagophore or autophagosome structures. Similar DAB-positive structures were also observed in HFT-PARK2^{WT};PINK1$^{-/-}$ cells reconstituted with PINK1-APEX2^{F} 1 hour after depolarization (fig. S1F).

Mitochondria-autophagosome synapse architecture discovery using autophagy receptor-driven proximity biotinylation

The MOM proximal localization of APEX2^{F}-OPTN on damaged mitochondria led us to use APEX2-based proteomics to identify

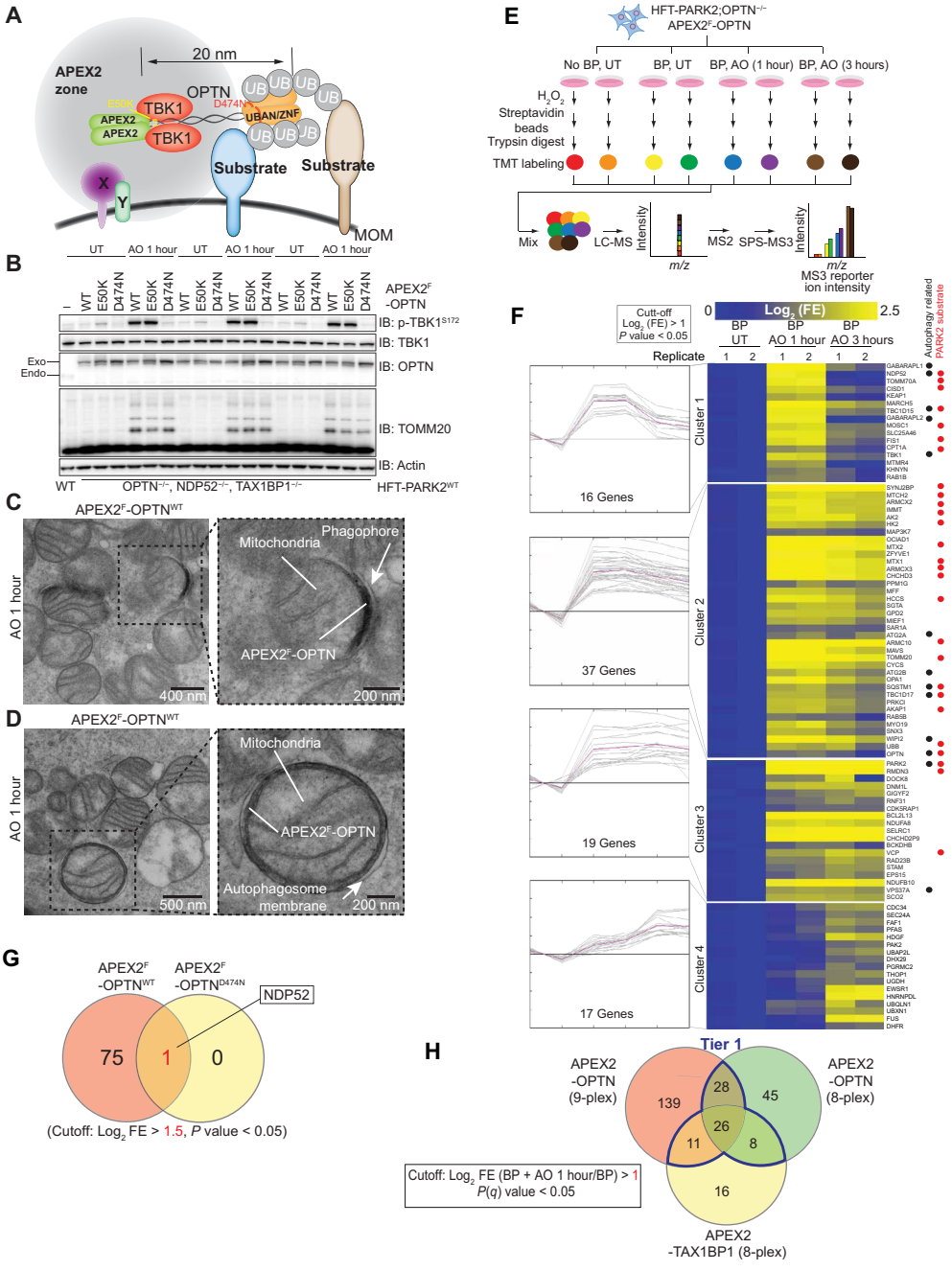

Fig. 1. Visualization and proteomic characterization of a depolarized mitochondria-autophagosome synapse using APEX2^{F}-OPTN. (**A**) Scheme depicting spatial analysis of APEX2^{F}-OPTN on the MOM. OPTN is depicted in an extended dimeric coiled-coil form with each UBAN domain in the dimer associated with two Ub molecules in a chain attached to a PARK2 substrate on the MOM. The proximity biotinylation zone is indicated by the gray sphere. The position of E50K and D474N mutations in OPTN is shown in yellow and orange, respectively. (**B**) HFT-PARK2^{WT};TKO;mt-Keima cells were reconstituted with WT, E50K, or D474N APEX2^{F}-OPTN, and these cells or the corresponding HFT-PARK^{WT} cells were left untreated or depolarized for 1 hour. Cell lysates were subjected to immunoblotting with the indicated antibodies. (**C** and **D**) EM analysis of depolarized (1 hour) APEX2-OPTN^{WT}–expressing cell thin sections after staining with DAB/H_2O_2 and osmium, which deposits an electron-rich signal where APEX2^{F}-OPTN is concentrated (*38*). Scale bars are indicated. (**E**) Scheme for 8-plex TMT analysis of proteins in proximity to APEX2^{F}-OPTN in response to mitochondrial depolarization. Duplicate cultures of HFT-PARK2^{WT};OPTN$^{-/-}$ cells expressing APEX2^{F}-OPTN^{WT} were left untreated, incubated with BP, or incubated with BP and AO (1 or 3 hours) before treatment with H_2O_2 (1 min). Cells were quenched and lysed in denaturing buffer, and biotinylated proteins were purified using streptavidin beads before on-bead trypsinization and TMT labeling. Mixed peptide samples were subjected to SPS-MS^3–based proteomics, and the intensity of TMT reporter ions for individual peptides was determined. (**F**) A heat map depicting four major clusters of proteins identified in the experiment outlined in (E) with $\log_2$ FC > 1.3 and –log (*P* value) > 2.0 is shown. Untreated samples are omitted from the heat map for simplicity. (**G**) Venn diagram of overlapping biotinylated proteins in proximity to either APEX2^{F}-OPTN^{WT} or APEX2^{F}-OPTN^{D474N}. (**H**) Venn diagram of proximity biotinylated proteins identified at 1 hour after depolarization in 9-plex (fig. S2, B to D) and 8-plex APEX2^{F}-OPTN^{WT} experiments and in the APEX2^{F}-TAX1BP1 experiment (fig. S2, G and H). Tier 1 proteins are found in two or more multiplexed experiments, while tier 2 proteins were found in a single experiment.

biotinylated proteins in close proximity to the synapse. Initially, we performed two independent experiments using HFT-PARK2^{WT};OPTN$^{-/-}$;APEX2^{F}-OPTN cells with or without depolarization and quantified biotinylated proteins isolated on streptavidin beads using tandem mass tagging (TMT) and synchronized precursor selection (SPS)-MS^3–based analysis of tryptic peptides (Fig. 1E) (*38*, *42*). First, we measured proximity biotinylation over a 1- or 3-hour time course of depolarization with AO using an 8-plex TMT work flow, with each condition in duplicate. This identified several dozen biotinylated proteins that were enriched at 1 and/or 3 hours after depolarization (dataset S1). K-means clustering of proteins that display changes in abundance [$\log_2$ fold change (FC) > 1.0; $P < 0.05$] identified four clusters containing 89 proteins (Fig. 1F). Clusters 1, 2, and 3 contained proteins whose biotinylation strongly increased at 1 hour and either was maintained at a similar level at 3 hours (cluster 3, 19 proteins) or was reduced to a variable extent at 3 hours (clusters 1 and 2, 53 proteins). Cluster 4 represents proteins whose biotinylation increased largely at 3 hours (17 proteins) (Fig. 1F). As described below, many of the proteins identified especially in clusters 1, 2, and 3 are linked with PARK2-dependent mitophagy. We then performed two parallel 9-plex TMT experiments examining APEX2^{F}-OPTN^{WT} and the APEX2^{F}-OPTN^{D474N} mutant that cannot bind Ub, with each condition in triplicate (Fig. 1G; fig. S2, B to F; and datasets S2 and S3). For OPTN^{WT}, we identified 76 biotinylated proteins that were enriched with depolarization, most of which were also seen in the 8-plex time course TMT experiment (Fig. 1H and fig. S2D). In contrast, the OPTN^{D474N} Ub binding mutant was enriched in only one protein (NDP52) [$\log_2$ FC > 1.5; $\log_{10}$ (P value) > 2] (Fig. 1G and fig. S2E). Thus, the vast majority of OPTN's proximity-dependent associations require its association with Ub chains on depolarized mitochondria. Last, as an independent approach for examining the mitochondrial-autophagosome synapse, we performed an 8-plex TMT experiment [including two channels for "no BP (biotin phenol)" controls] using HFT_PARK2^{WT};TKO cells reconstituted with APEX2^{F}-TAX1BP1, which is also recruited to damaged mitochondria (fig. S2, G and H, and dataset S4) (*9*). After 1 hour of depolarization, 61 proteins were found to be enriched in biotinylated samples ($\log_2$ FC > 1; $P < 0.05$), with a substantial fraction (73.7%) being identified in one or both TMT experiments with OPTN (Fig. 1H).

A proximity map of autophagy receptors on damaged mitochondria

In total, we identified 273 proteins as being selectively enriched in at least one of the three proximity biotinylation experiments with either OPTN or TAX1BP1. We organized these into tier 1 (73 proteins) based on identification in at least two of the three experiments and tier 2 (200 proteins) based on enrichment in only a single experiment ($P < 0.05$, $\log_2$ FC > 1) (Figs. 1H and 2, A and B). Gene Ontology (GO) analysis of tier 1 proteins revealed strong enrichment for cellular components and biological processes linked with mitophagy, autophagy, and mitochondrial fission, among other categories (fig. S2I). We assembled enriched proteins into modules representing functions associated with mitophagy (Fig. 2, A and B). First, 30 MOM or MOM-associated proteins previously shown to be ubiquitylated by PARK2 in response to depolarization in HeLa cells (*31*, *32*), including VDAC2, TOMM20, TOMM40, TOMM70A, HK2, SYNJ2BP, TBC1D15, HCCS, ARMC10, RMDN3 (also called FAM82A1), MFF, CHCHD3, MTCH2, IMMT, DNAJC11, ATAD1, MTX2, ATAD3B, NT5C3A, and CYB5R3, as well as PARK2 itself, were enriched (Fig. 2, A and B, and datasets S1, S2, and S4). Second, autophagy receptors NBR1, SQSTM1, and CALCOCO2/NDP52, as well as TBK1, were enriched (Fig. 2A). Biotinylation of distinct autophagy receptors by APEX2-tagged OPTN or alternatively by APEX2-tagged TAX1BP1 suggests that adaptors themselves are in close proximity with each other as they engage ubiquitylated proteins on the MOM (see below). Third, multiple proteins linked with autophagosome production were enriched, including GABARAP, ATG3, and WIPI2, indicating that OPTN comes in proximity to autophagosome/phagophore machinery, which is also indicated by DAB staining (Figs. 1C and 2A). Fourth, a number of proteins linked with vesicle fusion including RAB7A, previously reported to be recruited to depolarize mitochondria and to promote mitophagy (*43*, *44*), as well as RAB1A/B, RAB8A, SNX3, and TSG101 were enriched in either tier 1 or tier 2 proteins (Fig. 2A).

Validation of candidate proteins enriched at the mitochondria-autophagosome synapse

Three further approaches were used to validate these findings. First, we used label-free proteomics to independently measure protein abundance in mitochondria and found that the identity of proteins identified by APEX2 was distributed widely across the mitochondrial proteome abundance (Fig. 2C). This indicates that the abundance of the protein on the MOM is not a major determinant of the extent of proximity biotinylation and serves as a measure of specificity. Second, HFT_PARK2^{WT};OPTN$^{-/-}$ cells expressing APEX2^{F}-OPTN at endogenous levels were either left untreated or depolarized for 1 hour in the presence of BP for proximity biotinylation. Proteins were purified using immobilized streptavidin, and immunoblots were probed for candidate proximity-labeled proteins (Fig. 2D). All candidates were enriched in streptavidin-purified proteins in response to depolarization, confirming the proteomic data. Third, we validated two candidates at the ultrastructural level. HFT_PARK2^{WT};WIPI2$^{-/-}$ cells were reconstituted with APEX2^{F}-WIPI2 (isoform 1) and used in combination with DAB staining and EM of thin sections to reveal electron dense staining for APEX2^{F}-WIPI2 on the surface of mitochondria in depolarized cells, frequently juxtaposed by autophagosomal membranes (Fig. 2E). Similarly, HFT_PARK2^{WT};RAB7$^{-/-}$ cells reconstituted with APEX2^{F}-RAB7A display DAB staining juxtaposed between damaged mitochondria and autophagosome by EM (Fig. 2F), consistent with RAB7A recruitment to damaged mitochondria (*43*, *44*). Together, these data confirm the close association of mitophagy cargo receptors with a large number of proteins on the MOM and proteins traditionally thought of as being associated with the growing autophagosome (Fig. 2, A and B).

Focused CRISPR-Cas9 screens define the genetic landscape of mitophagic flux

The experiments described above begin to provide a molecular roadmap describing the landscape of proteins at the synapse between damaged mitochondria and the autophagosome/phagophore. Among the proteins identified are proteins with no known link in the mitophagy process. We therefore sought to complement the proteomic approach with genetic identification of potential regulators of the process, potentially including a wide cross section of genes encoding proteins that are enriched at the synapse. To develop a strategy for genetic analysis of mitophagic flux, we turned to mt-mKeima, a mitochondrial matrix–targeted pH-responsive reporter that undergoes a chromophore resting charge state change upon trafficking to the lysosome (pH of ~4.5) (*45*, *46*). This system allows mitophagy flux measurements to be

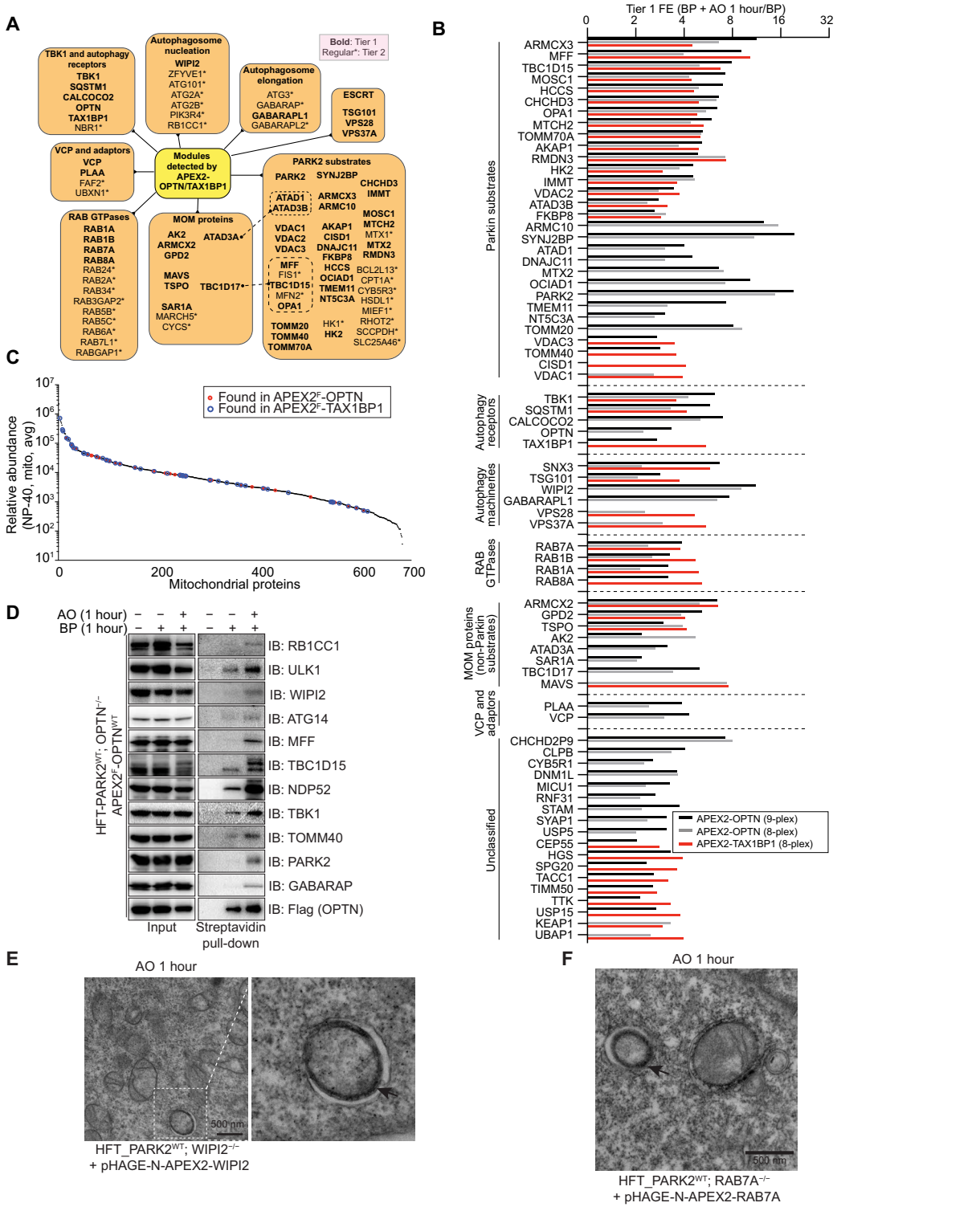

Fig. 2. A proximity map of autophagy receptors on damaged mitochondria. (**A**) Overview of tier 1 and tier 2 biotinylated proteins identified with APEX2^{F}-OPTN and APEX2^{F}-TAX1BP1. Tier 1 proteins are identified in at least two experiments, while tier 1 proteins were identified in only a single experiment. GTPase, guanosine triphosphatase. (**B**) Tier 1 protein fold enrichment (FE) classified according to roles for proteins in PARK2-dependent mitophagy. (**C**) HFT-PARK2^{WT};OPTN$^{-/-}$ cells expressing APEX2^{F}-OPTN^{WT} were left untreated, incubated with BP, or incubated with BP and AO (1 hour) before treatment with H_2O_2 (1 min). Cell extracts were either immunoblotted directly or used for streptavidin pull-downs, followed by immunoblotting with the indicated antibodies. (**D**) Rank of individual biotinylated proteins identified with OPTN or TAX1BP1 according to the relative abundance of 700 mitochondrial proteins measured by label-free mass spectrometry. (**E**) HFT_PARK2^{WT};WIPI2$^{-/-}$ cells stably expressing APEX2-WIPI2 were depolarized for 1 hour, and processes for DAB/osmium staining were followed by EM of thin sections. (**F**) HFT_PARK2^{WT};RAB7A$^{-/-}$ cells stably expressing APEX2-RAB7A were depolarized for 1 hour, and processes for DAB/osmium staining were followed by EM of thin sections.

performed by flow cytometry. We first benchmarked a flow cytometry–based mt-mKeima flux assay that measures the mean emission intensity ratio at 620 nm (excitation of 561 nm/excitation of 488 nm) using HFT_PARK2^{WT} or catalytically defective PARK2^{C431S} with or without deletion of known mitophagy components. As expected (*9*), phosphorylation of TBK1^{S172} in response to AO (1 hour) was eliminated in TKO cells lacking OPTN, NDP52, and TAX1BP1, as was mitophagy at 33 hours after depolarization as quantified using a conventional mitochondrial DNA staining method as previously described (fig. S3, A and B) (*25*). We then used mt-mKeima to monitor flux at 16 hours after depolarization by flow cytometry, observing a ~2.5-fold increase in mitophagic flux at 16 hours after depolarization (fig. S3, C and D). This increase was dependent on PARK2 and PINK1 and was largely or fully blocked in TKO cells, in cells lacking TBK1, or in some (but not all) patient-associated PINK1 mutations reconstituted into PINK1$^{-/-}$ mt-mKeima reporter cells (fig. S3, D to F). Similar results were observed at 6 hours after depolarization, albeit with a smaller dynamic range (fig. S3G).

Having demonstrated that this mitophagic flux assay faithfully recapitulated known genetic requirements for PARK2 and PINK1-driven mitophagy, we then infected HFT-PARK2^{WT};mt-mKeima reporter cells with one of three custom CRISPR-Cas9 KO libraries targeting ~700 "autophagy and vesicle trafficking genes" (which includes a variety of genes linked with vesicle transport, endocytosis, RAB signaling, lysosomal transport), ~1090 resident mitochondrial proteins, or ~850 components of the Ub-like (UbL) protein conjugation (E2s and E3s) and deconjugation machinery (Fig. 3A and dataset S5). Each library was designed to have ~10 gRNAs per gene and was infected with a representation of >500 and a multiplicity of infection (MOI) of 0.2 (see Materials and Methods). After selection for 7 days to allow for gene inactivation, cells were supplemented with doxycycline (2.5 hours) to induce low-level PARK2^{WT} expression and depolarized for 16 hours (in the absence of doxycycline, before sorting for cells with high or low mt-mKeima signal; Fig. 3A). In some experiments, cells were also sorted 4 hours after depolarization. gRNA barcodes from cells with high (4-hour time point) or low (16-hour time point) mKeima signals were sequenced by next-generation sequencing, and enriched gRNA barcodes were identified using the MAGeCK (Model-based Analysis of Genome-wide CRISPR-Cas9 Knockout) algorithm (Fig. 3A) (*47*).

As an initial indication of screen performance for positive regulators of mitophagic flux, we found that gRNAs targeting either PARK2 or PINK1 were among the most highly enriched in cells infected with the autophagy and trafficking library, consistent with their central role in the pathway (Fig. 3B and dataset S5). Moreover, PARK2 was identified as the strongest positive regulator from the Ub-like pathway library, and PINK1 was similarly identified as the strongest scoring gene in the resident mitochondrial protein library (Fig. 3, C and D, and dataset S5). Among the most highly enriched genes [MAGeCK scores: $\log_2$ FE > 0.5 and false discovery rate (FDR) < 0.05] were components previously linked with several core autophagic modules, including the following: (i) proteins involved in phosphoinositide 3-phosphate (PI3P) production and recognition, including all four core subunits of the VPS34 kinase complex and WIPI (WD40 repeat protein interacting with phosphoinositides) proteins, which bind PI3P on the growing phagophore; (ii) proteins involved in ATG8 maturation and conjugation to PE; (iii) proteins involved in autophagosomal vesicle formation and/or fusion, including both the TRAPPC (trafficking protein particle complex) and HOmotypic fusion and vacuole Protein Sorting (HOPS) complexes (*48*–*52*); (iv) regulatory components of the ULK1 or ULK2 kinase complex involved in the initiation of phagophore formation (*53*, *54*); and (v) the TOMM7 protein previously linked with stabilization of PINK1 on depolarized mitochondria (Fig. 3, B to F) (*55*). gRNAs targeting OPTN were also enriched but with a MAGeCK score of 0.31 ($P < 0.02$), consistent with NDP52 and TAX1BP1 being at least partially redundant (dataset S5) (*9*, *10*). In addition, several genes not specifically linked previously with mitophagy were also identified, including several whose functions are associated with membrane trafficking or that were also enriched at the mitochondrial-autophagosome synapse as described below (Fig. 1, E and F, and dataset S5).

Because of the very high proportion of cells undergoing mitophagy 16 hours after depolarization, it is possible to score even a small fraction of cells within a pool of CRISPR-Cas9–expressing cells that have successfully deleted a gene critical to mitophagic flux. As an initial validation step, we created two new gRNAs targeting 11 candidates from the initial screens along with a control gRNA-targeting green fluorescent protein (GFP), cloned these into the identical lentiviral Cas9 vector system used for the library generation, and infected HFT_PARK2^{WT};mt-Keima cells. After 7 days to allow for gene inactivation, we depolarized cells for 16 hours and measured mitophagic flux by flow cytometry (Fig. 3G). In cells expressing the GFP gRNA, only 5% of cells were negative for lysosomal Keima fluorescence. In contrast, >20 to 40% of cells harboring gRNAs for TRAPPC4, WIPI2, and ATG9A were negative for lysosomal mKeima fluorescence, indicating a block to mitophagic flux. Several other candidates displayed >5 to 15% of cells that were mKeima negative, indicating a partial defect in mitophagic flux (Fig. 3G). Moreover, we used CRISPR-Cas9 to create deletions in several candidate genes and isolated single-cell HFT-PARK2^{WT} clones before performing mitophagy assays using a complementary method. Cells expressing PARK2 were depolarized for 32 hours, and mitochondrial DNA content was measured by immunofluorescence, assessing the number of cells with unaggregated, aggregated, or cleared mitochondria (fig. S3H), as described previously (*25*). Previous studies have indicated that mitochondrial fragmentation and aggregation occur rapidly upon depolarization and are followed by a much slower turnover of mitochondria (*29*, *41*). For all cases examined with the exception of TBC1D15, the number of cells with cleared mitochondria was reduced, with HK2$^{-/-}$, SEC22B$^{-/-}$, and WIPI2$^{-/-}$ cells displaying the largest reduction in cleared mitochondria (fig. S3H). However, the extent of aggregation varied significantly among candidate genes, as addressed further below. gRNAs targeting a number of mitochondrial components including the translocon, the mitoribosome, RNA polymerase (POLRMT), the fission-fusion cycle (FIS1, MFN2), and the porin VDAC1, among others, were enriched in cells with increased mitophagic flux 4 hours after depolarization (Fig. 3H and fig. S3I). Increased flux in this case could reflect either sensitization to depolarization or increased mitochondrial dysfunction and PARK2-dependent mitophagy under basal conditions. Consistent with the latter interpretation, we observed enhanced mitophagic flux in cells harboring deletions of VDAC1/2, or VDAC1/TOMM70A under basal conditions using the mt-mKeima assay (fig. S3J).

Proteogenetic landscape of PARK2-dependent mitophagy

PARK2-dependent mitophagy involves a number of functional modules, including the general autophagy machinery involved in phagophore nucleation (the PIK3C3/VPS34 complex and the

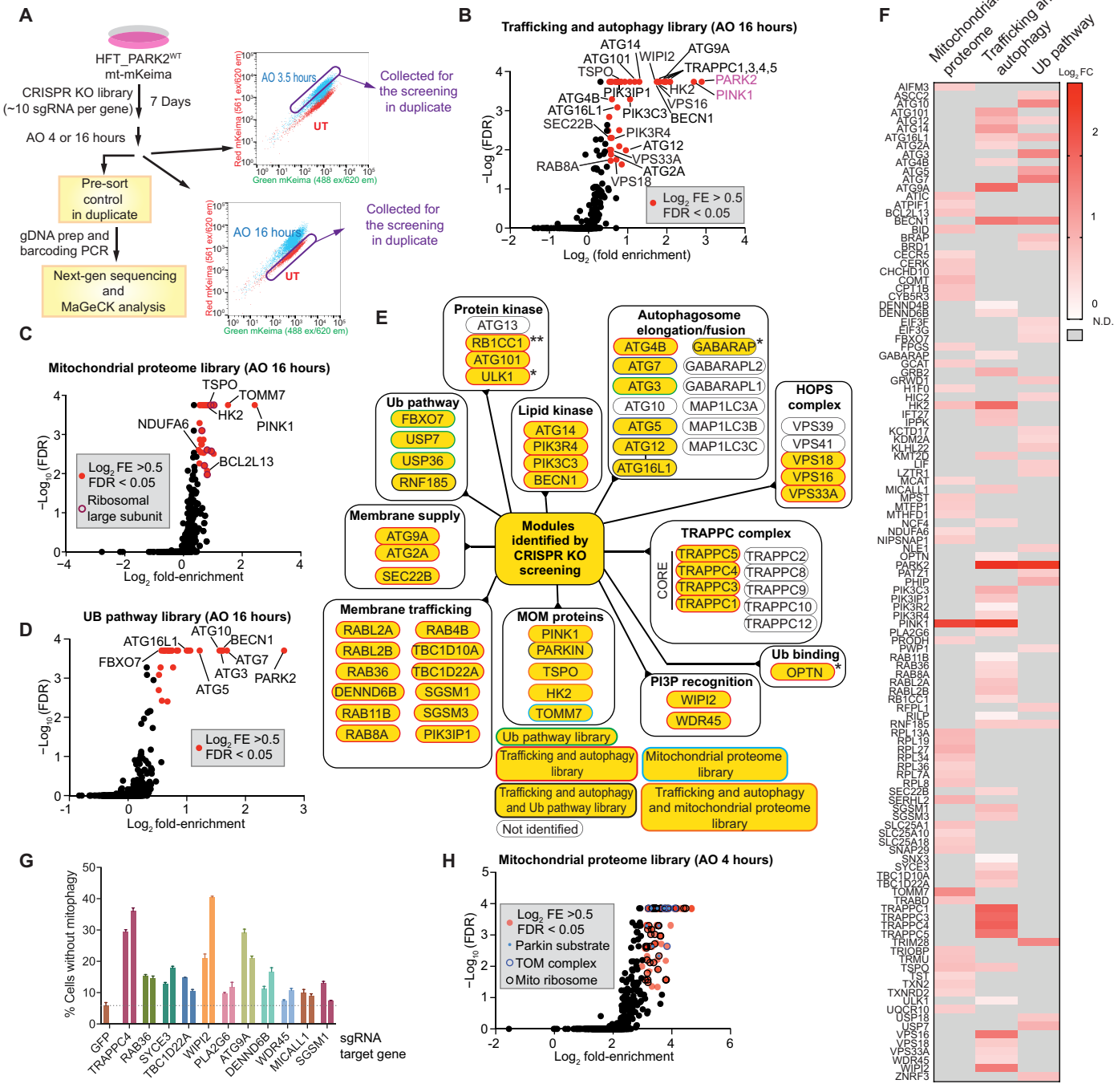

Fig. 3. A screen for mitophagic flux regulators identifies the genetic landscape for mitophagy. (**A**) Schematic outline of the mitophagic flux CRISPR-Cas9 screen. Duplicate cultures of HFT-PARK2 cells expressing mt-Keima were infected with one of three pathway-focused gRNA libraries (trafficking and autophagy, mitochondrial proteome, or Ub pathway). PARK2 expression was induced, and cells were depolarized for 16 hours before sorting on the basis of mean emission intensity ratio at 620 nm (excitation 561 nm/excitation 488 nm). PCRed barcodes from sorted cells were subjected to sequencing and MAGeCK analysis. (**B** to **D**) Plots of MAGeCK scores [−log (FDR) versus $\log_2$ (FE)] for genes identified in trafficking and autophagy (B), mitochondrial proteome (C), and Ub pathway (D) screens. Red dots indicate candidate genes with $\log_2$ FE > 0.5 and FDR < 0.05. (**E**) Modules and functional classes of candidate genes identified in CRISPR-Cas9 screens for mitophagic flux. Genes in yellow are identified in the screen. Genes indicated with a single or double asterisk were enriched with a $\log_2$ FC of >0.28 or had a −log (FDR) of 0.05, respectively. (**F**) Heat map for candidate genes identified in each of the three CRISPR-Cas9 libraries used. Genes not detected (N.D.) with $\log_2$ FE > 0.5 are shown in gray. (**G**) Validation screen for candidate identified from primary screens. (**H**) A screen for identification of genes whose depletion increases mitophagic flux. As in (B) but with sorting at 4 hours after depolarization.

ULK1-FIP200 complex), ATG8 lipidation, and vesicle fusion machinery (TRAPPC, HOPS complex, RAB guanosine triphosphatases, and ESCRT-I), as well as components of the PARK2 activation system and Ub-binding autophagy receptors, which couple with the autophagy machinery (*8*, *15*). Our proximity proteomics and genetic experiments identified components across all modules of the pathway while also identifying potential new components (Fig. 4). In total, 7.3% of the proteins identified as enriched at the mitochondrial-autophagosome/phagophore synapse were also identified by CRISPR screens. First, components of the phagophore nucleation machinery and ATG8 conjugation system were strongly enriched genetically, as expected, but we also identified several of these components in proximity to mitophagy receptors, including WIPI2, ATG2A, FIP200, GABARAPs, and ATG3. FIP200 has recently been shown to physically associate with cargo receptors, including NDP52, explaining the observed proximity (*12*, *14*). Although we did not identify peptides for ULK1 or ATG14 (a component of the VPS34 complex) by proximity biotinylation, we did detect their enrichment in APEX2^{F}-OPTN experiments by immunoblotting (Fig. 2D). Second, a number of known PARK2 ubiquitylation targets or MOM proteins enriched in proximity biotinylation experiments were also identified in CRISPR-Cas9 KO library screens and, in some cases, validated by independent deletion and mitophagy analysis (fig. S3H), including TSPO (a multipass transmembrane MOM protein not previously linked with mitophagy), BCL2L13, and HK2, as further analyzed below. Third, while the HOPS complex and the associated SNARE SNAP29 were identified via CRISPR-Cas9 KO library screening, they were not enriched in the APEX2^{F}-OPTN or TAX1BP1 experiments, consistent with their

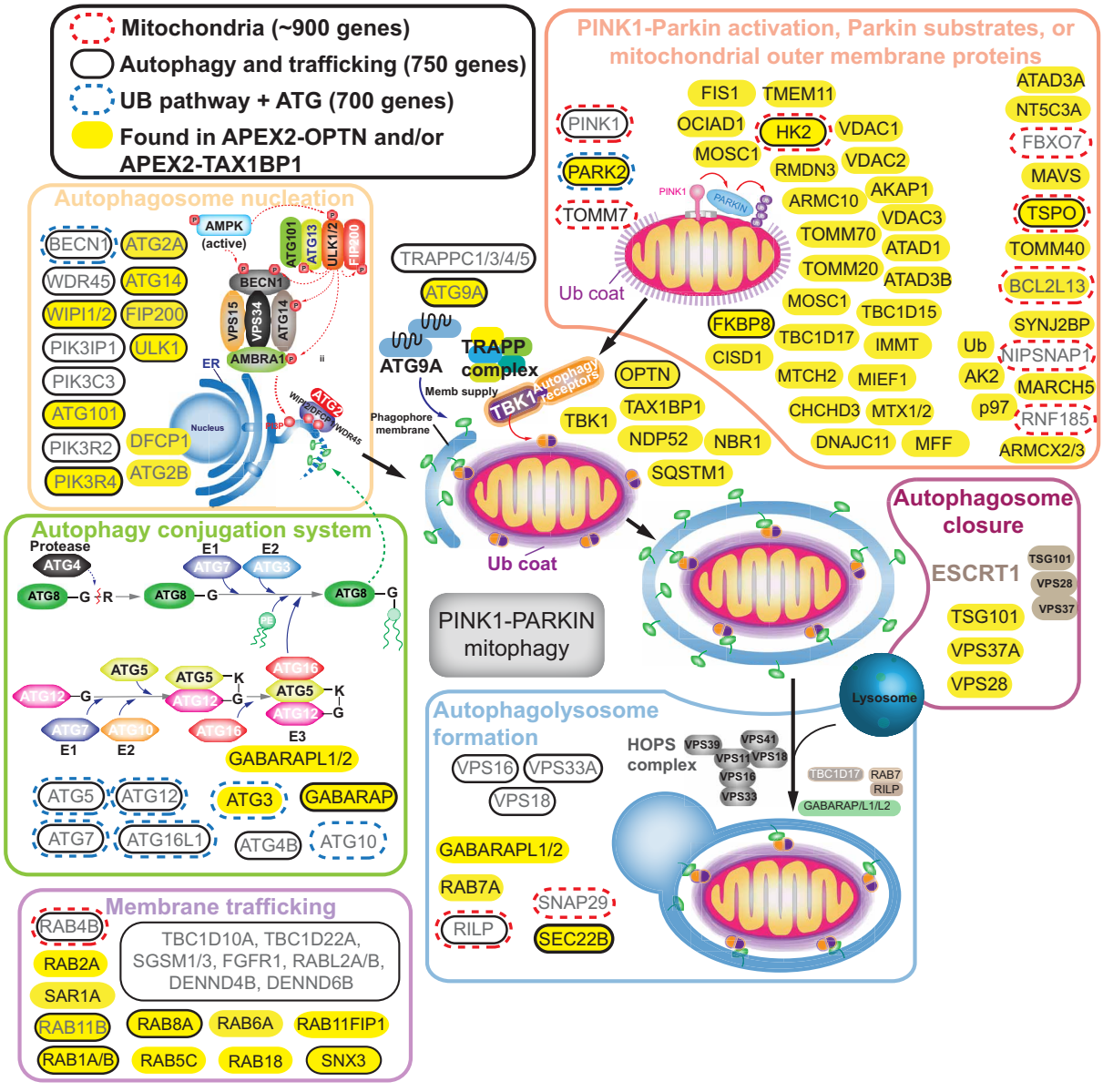

Fig. 4. Proteogenetic landscape of PARK2-dependent mitophagy. A summary of functional modules involved in autophagy and trafficking of damaged mitochondria for mitophagy is shown with individual components identified in one of the three CRISPR-Cas9 screens or by proximity biotinylation with either APEX2^{F}-OPTN or APEX2^{F}-TAX1BP1 indicated as shown in the legend.

interaction with fully closed autophagosomes to promote lysosomal fusion (*56*). In contrast, other vesicle fusion/trafficking machinery, including RAB7A known to be involved in mitophagy (*43*, *44*) as well as components of ESCRT-I involved in autophagosomal closure (*57*, *58*), were enriched in the proximity biotinylation experiments, indicating that they play roles at the mitochondrial-autophagosome synapse (Fig. 4). This integrated proteogenetic landscape of PARK2-dependent mitophagy serves as a resource for the identification of additional components in the pathway (see Discussion).

HK2 localizes at the mitochondria-autophagosome synapse

PARK2-dependent mitophagy occurs in several steps that can be assessed by examining the biochemical activities of individual components, potentially allowing the points of action of any individual pathway component to be interrogated (*8*). To evaluate the potential of the proteogenetic landscape to provide additional mechanistic insight, we examined HK2. HK2 is associated with the MOM, in part by interaction with VDAC proteins (*37*), and is a known substrate of PARK2 in response to mitochondrial depolarization (*31*–*33*). In addition, a previous study suggested the involvement of HK2 activity in recruitment of PARK2 to mitochondria through an unknown mechanism (*59*). Consistent with proximity biotinylation of HK2 by APEX2^{F}-OPTN and TAX1BP1, HFT_PARK2^{WT};HK2$^{-/-}$ cells reconstituted with HK2-APEX2^{F} revealed electron-rich DAB staining between the MOM and an autophagosome encircling the mitochondria 1 hour after depolarization (Fig. 5A). This HK2-APEX2^{F} protein was able to largely rescue defects on PARK2-dependent mitophagic flux in HK2$^{-/-}$ cells (Fig. 5B).

HK2, but not HK1, promotes accumulation of pS65-Ub on damaged mitochondria

We next examined the role of HK2 in the early steps of PINK1-PARK2 activation. As expected, we observed robust accumulation of pS65-Ub in either whole-cell extracts (WCEs) or crude mitochondrial lysates 1 hour after depolarization with AO (Fig. 5, C and D, lane 1 versus lane 4). In contrast, HK2$^{-/-}$ cells, but not HK2$^{-/-}$ cells reconstituted with HK2-APEX2, displayed markedly reduced levels of pS65-Ub when assayed immediately after clonal expansion of cells, suggesting a defect in either PINK1 activation or accumulation of Ub chains that then serve as substrates for PINK1 (Fig. 5, C and D, lane 5 versus lane 6). Ubiquitylation of known PARK2 substrates TOMM20 and CISD1 was largely unaffected in HK2$^{-/-}$ cells, as was the accumulation of Ub chains in response to depolarization (Fig. 5, C and D). HK1, a paralog of HK2, is also ubiquitylated in response to PARK2 activation (*31*–*33*) and was detected in proximity with OPTN (Fig. 2A). However, HK1$^{-/-}$ cells had no detectable effect on depolarization-dependent formation of pS65-Ub or TOMM20 ubiquitylation in either WCEs or crude mitochondria (Fig. 5, E and F), and mitophagy was largely unaffected by HK1 deletion (fig. S4A). HK2 deletion did not affect mitochondrial membrane potential as measured by JC-1 staining, with or without depolarization, nor did HK2 deletion alter intracellular adenosine triphosphate (ATP) levels, charging of the ATP-dependent Ub-activating enzyme (UBA6), or glucose-6-phosphate levels 1 hour after depolarization, although we did observe a reduction in ATP levels in HK2$^{-/-}$ cells after longer periods of depolarization (29 hours) (fig. S4, B to E). These data suggest that defects in pS65-Ub accumulation seen in HK2$^{-/-}$ cells are not a direct effect of alterations in cellular energetics. The ability of HK2-APEX2^{F} to rescue pS65-Ub accumulation in HK2$^{-/-}$ cells did not require hexokinase catalytic activity (kinase dead mutant) or phosphorylation on T473, a known site of Akt-dependent phosphorylation (Fig. 5G). Moreover, mutation of three major sites of HK2 ubiquitylation by PARK2 (K176, K323, and K337) to Arg had no effect on the ability of HK2 to rescue pS65-Ub phosphorylation in HK2$^{-/-}$ cells (Fig. 5H). Upon extensive expansion of HK2$^{-/-}$ cells (>2 months), we observed multiple effects consistent with a form of cellular adaptation, including reduced depolarization-dependent accumulation of PINK1, a more marked reduction in the accumulation of pS65-Ub, and a more marked reduction in PARK2 recruitment, as well as TOMM20 ubiquitylation (fig. S4F). This suggests that care must be taken in analyzing phenotypes with cells lacking HK2.

HK2 promotes formation of a ~700-kDa PINK1 complex to facilitate S65-Ub phosphorylation

The reduced level of pS65-Ub in depolarized HK2$^{-/-}$ cells in the absence of overt changes in primary substrate ubiquitylation by PARK2 led us to examine PINK1. PINK1 is markedly stabilized upon mitochondrial depolarization, where it forms a complex with the mitochondrial translocon (*17*, *18*). However, across several experiments, we saw no effect on the accumulation of total PINK1 protein in the absence of HK2 in either WCEs or purified mitochondria, as assessed by SDS–polyacrylamide gel electrophoresis (PAGE) (Fig. 5, D, F, and G). We therefore examined the ability of PINK1 to assemble into high–molecular weight complexes with the translocon using blue native (BN)–PAGE. One hour after depolarization—the earliest time point where pS65-Ub is maximal (*24*)—the majority (70%) of PINK1 in mitochondria accumulated in a ~700-kDa complex, with a smaller fraction (30%) migrating at ~66 kDa (approximating the size of monomeric PINK1) (Fig. 5I). In contrast, PINK1 was not detected in native gel analysis in the absence of depolarization, consistent with its rapid turnover in cells with healthy mitochondria (*17*). A fraction of PARK2 (27%) could be observed in a ~700-kDa complex, although the majority of PARK2 remained at a molecular weight approximating the monomeric protein (Fig. 5I). In contrast, much smaller amounts of PINK1 accumulate in the ~700-kDa complex in HK2$^{-/-}$ cells, and there was a concomitant reduction in the amount of PARK2 in the ~700-kDa complex (Fig. 5, I and J). These defects were rescued by HK2-APEX2^{F} (Fig. 5, I and J). The accumulation of PARK2 in the ~700-kDa complex with PINK1 was fully dependent on PINK1 activity, as two patient-based PINK1 mutants (A168P and E240K) that fail to activate PARK2 or phosphorylate Ub (fig. S4G) also fail to accumulate PARK2 in the ~700-kDa complex (fig. S4G). Together, these data indicate a potential scaffolding role for HK2 that facilitates its assembly into a ~700-kDa complex with the translocon.

DISCUSSION

In this study, we used proximity biotinylation together with focused genetic screens for mitophagic flux to examine the landscape of OPTN-dependent and PARK2-dependent mitophagy. APEX2-driven proximity biotinylation provides a way to identify proteins that are within ~10 nm of the APEX2 domain and, when used in conjunction with quantitative proteomics approaches, as described here, can provide information concerning local protein assemblies on membrane surfaces, as well as how these interactions are altered in response to specific signals (*60*). We found that APEX2-OPTN is highly concentrated at the mitochondria-autophagosome synapse with 1 hour of mitochondrial depolarization, based on EM of cell thin sections,

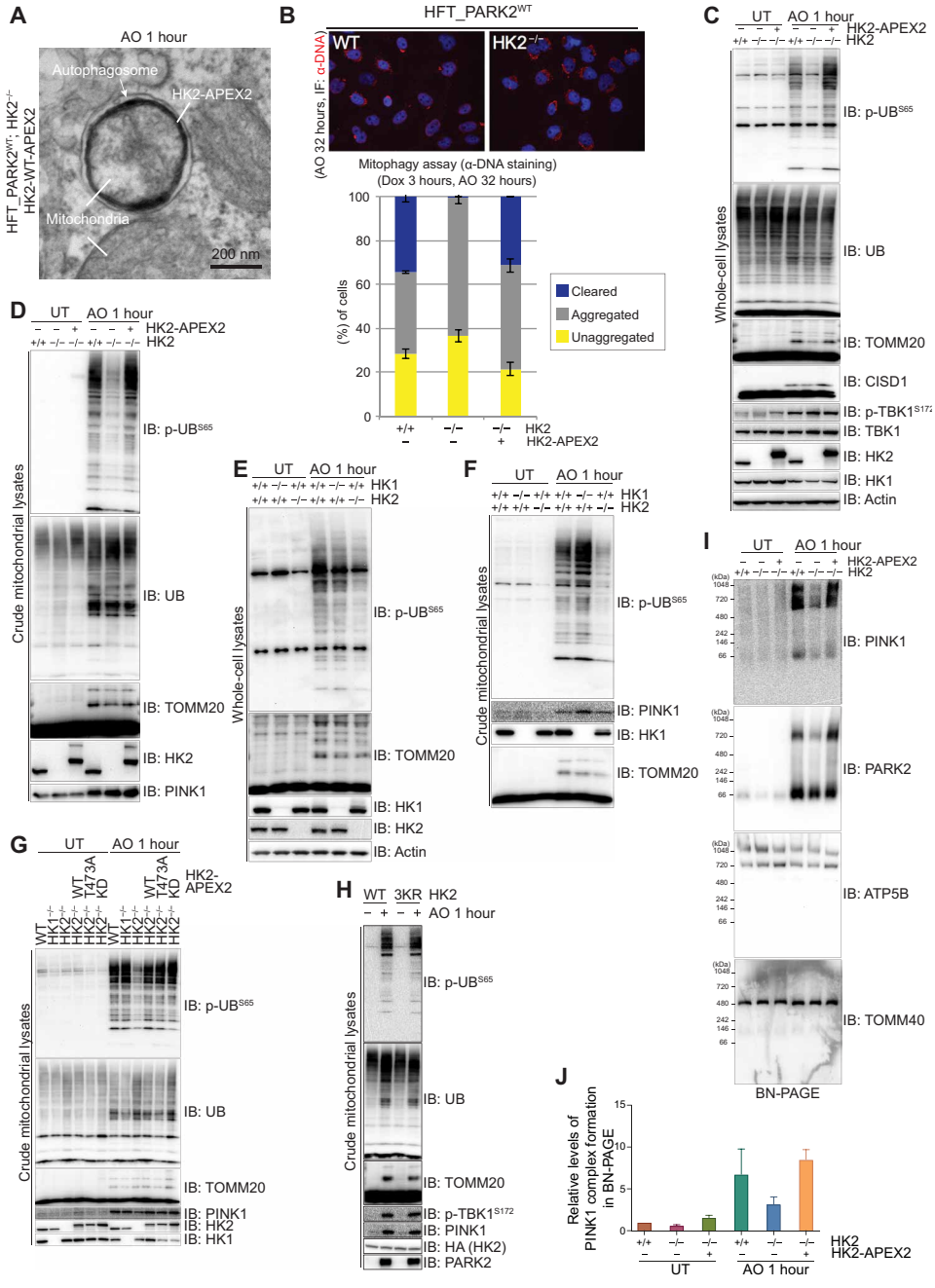

Fig. 5. HK2, but not HK1, promotes assembly of PINK1 with the mitochondrial translocon and its activation upon mitochondrial depolarization. (**A**) HFT_PARK2^{WT};HK2$^{-/-}$ cells stably reconstituted with HK2-APEX2 were depolarized with AO (1 hour) and subjected to staining with DAB/H_2O_2 and osmium, which deposits an electron-rich signal where HK2-APEX2 is concentrated. Sections were then analyzed by EM. Scale bars are indicated. (**B**) The indicated cells (HFT-PARK2^{WT}, HFT-PARK2^{WT};HK2$^{-/-}$, and HFT-PARK2^{WT};HK2$^{-/-}$ expressing HK2-APEX2^{F}) were subjected to depolarization for 32 hours, and mitochondrial DNA was stained with α-DNA antibody in biological triplicate. More than 100 cells were classified and quantified (mean ± SEM) as having unaggregated mitochondria, aggregated mitochondria, or mitochondria cleared by mitophagy. Dox, doxycycline. (**C** and **D**) The indicated HFT-PARK2^{WT}, HFT-PARK2^{WT};HK2$^{-/-}$, and HFT-PARK2^{WT};HK2$^{-/-}$ expressing HK2-APEX2^{F} were either left untreated or treated with AO (1 hour). Whole-cell lysates (C) or purified mitochondria (D) were immunoblotted using the indicated antibodies. (**E**) The indicated HFT-PARK2^{WT}, HFT-PARK2^{WT};HK1$^{-/-}$, and HFT-PARK2^{WT};HK2$^{-/-}$ cell lines were either left untreated or treated with AO (1 hour) before immunoblotting as in (C). (**F**) Mitochondria isolated from cells in (E) were subjected to immunoblotting with indicated antibodies. (**G**) The indicated HFT-PARK2^{WT}, HFT-PARK2^{WT};HK1$^{-/-}$, HFT-PARK2^{WT};HK2$^{-/-}$, and HFT-PARK2^{WT};HK2$^{-/-}$ cells reconstituted with either HK2^{WT}, HK2^{T473A}, or HK2^{KD}-APEX2^{F} were either left untreated or treated with AO (1 hour) and crude mitochondria immunoblotted with indicated antibodies. KD, kinase dead mutant. (**H**) The indicated HFT-PARK2^{WT};HK2$^{-/-}$ cells reconstituted with either HK2^{WT} or HK2$^{3KR\ (K176R,\ K323R,\ K337R)}$-APEX2^{F} were either left untreated or treated with AO (1 hour), and purified mitochondria were immunoblotted with the indicated antibodies. (**I**) Mitochondria isolated from the indicated HFT-PARK2^{WT}, HFT-PARK2^{WT};HK2$^{-/-}$, and HFT-PARK2^{WT};HK2$^{-/-}$ expressing HK2-APEX2^{F} cell lines were solubilized and subjected to BN-PAGE followed by immunoblotting with indicated antibodies. (**J**) Quantification of high–molecular weight PINK1 complex as in (H) by densitometry analysis (ImageJ) from biological triplicate experiments (mean ± SEM).

and in some cases, we detect early phagophore structures in close proximity to APEX2-OPTN (30%). This dynamic association with damaged mitochondria explains the appearance of foci on a subset of individual mitochondria using immunofluorescence to detect cargo receptors (*9*, *10*). We observed distances of ~25 to 50 nm between the MOM and the autophagosome/phagophore. In this regard, OPTN in an extended conformation is expected to be ~20 nm (Fig. 1A), suggesting that a plausible model in which association between OPTN and ubiquitylated proteins on the MOM, on the one hand, and OPTN and either ATG8 proteins (*61*) or the ULK1-RB1CC1 complex, on the other hand (*12*, *14*), would allow templating of the autophagosome/phagophore nearby the ubiquitylated MOM (Fig. 6A). This is consistent with the idea that OPTN functions as a molecular tether linking ubiquitylated cargo to the autophagy machinery.

A major unanswered question concerns the extent to which individual proteins that are targeted for ubiquitylation by PARK2 are used to selectively recruit OPTN and other cargo adaptors to the MOM. We found that a host of PARK2 targets on the MOM are detected in proximity with OPTN, and this requires that OPTN be able to bind Ub (Figs. 2A and 6A). First, we observed enrichment of other mitophagy cargo receptors (NDP52/CALCOCO2 and TAX1BP1) in APEX2-OPTN biotinylation products, and likewise, SQSTM1 and NBR1 enriched with APEX2-TAX1BP1. These close interactions could occur by each individual adaptor being associated with the same Ub chain, distinct Ub chains on the same PARK2 target molecule, or Ub chains on distinct proteins that are located very close to each other on the MOM (Fig. 6A). Currently, the extent to which individual PARK2 substrates have chains as opposed to monoubiquitylation is not clear, and as such, the precise interactions necessary for Ub-binding receptor recruitment are not clear (*8*). As such, it remains an open question as to whether there are sufficiently long chains to recruit multiple receptors to the same chain to generate sufficient receptor density for autophagosome/phagophore assembly. Nevertheless, the close proximity of receptors that allows trans-biotinylation suggests dense packing of receptors on the MOM. Second, we observed enrichment of multiple components of the translocon (TOMM70, TOMM20, and TOMM40) where PINK1 is known to be stabilized (*18*), and TOMM20, TOMM40, and TOMM70 have been identified as PARK2 targets (*31*, *32*, *62*). A number of other PARK2 substrates and MOM proteins are also enriched with both OPTN and TAX1BP1 (Figs. 2A and 4). Third, APEX2 receptors were enriched in components that are known to either nucleate or be localized at the autophagosome/phagophore, including components of the VPS34-PIK3R4-ATG14 complex (PIK3R4, ATG14) that marks the phagophore with PI3P; WIPI2, which binds PI3P on the phagophore; ATG8 proteins (particularly GABARAPL1), which are incorporated into the autophagosome/phagophore membrane; and ULK1-RB1CC1, which associates with the receptors themselves and also with autophagy machinery on the autophagosome/phagophore (Fig. 6A) (*12*, *14*). Given the variety of MOM proteins identified in proximity to OPTN or TAX1BP1, it would appear as though there is not one or a small number of PARK2 substrates that serve as a predominant or specialized target for recognition by the Ub-binding receptors but that receptors may bind largely in a manner that is agnostic of the ubiquitylated protein itself. Although it seemed possible that Ub density on the MOM could be a major feature driving mitophagy, it would appear that a number of PARK2 substrates that are far less abundant than VDACs, which themselves are among the most abundant proteins on the MOM (*33*), are nonetheless enriched in proximity biotinylation experiments with either OPTN or TAX1BP1 (Fig. 2C).

To complement these biochemical experiments, we performed genetic screens for mitophagic flux using libraries targeting ~2400 genes linked with autophagy and trafficking, the Ub system, and proteins localized in mitochondria. In addition to numerous known components of core autophagy machinery, we also identified candidates with no known roles in mitophagy (Fig. 4), several of which were confirmed by follow-up genetic validation. Among the strongest candidates from the genetic screen was HK2, a PARK2 substrate that associates with VDAC proteins (*32*, *33*, *37*). Previous studies using RNA interference suggested a role for HK2 in recruitment of PARK2 to damaged mitochondria (*59*). We generated cells lacking HK2, and the related enzyme HK1, and found strong blockade of mitochondrial clearance in HK2$^{-/-}$, but not HK1$^{-/-}$, cells in response to depolarization (Fig. 5B). Mechanistically, HK2 was found to be enriched at the mitochondrial synapse on the basis of APEX2

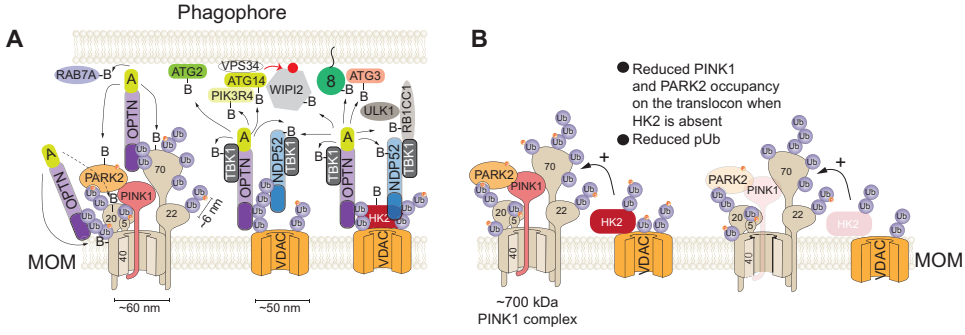

Fig. 6. Landscape of the mitochondria-autophagosome synapse. (**A**) A schematic depicting a subset of proteins identified by proximity biotinylation is shown. OPTN, a Ub-binding receptor for mitophagy, associates with Ub via its C-terminal UBAN domain (dark blue) and is thought to interact minimally with a di-Ub moiety. OPTN is a coiled-coil dimeric protein and is expected to be ~20 nm in a fully extended conformation. Recruitment of APEX2-tagged OPTN to ubiquitylated PARK2 targets on the MOM allows the identification of proteins located nearby (within ~10 nm of the APEX2 domain). Biotinylated proteins identified by quantitative mass spectrometry are indicated with a "B." The autophagosome/phagophore is recruited nearby the MOM (within ~25 to 50 nm). The approximate sizes of the TOMM40 component of the translocon, the VDAC proteins, and dimeric Ub are shown. (**B**) Schematic showing the potential role of HK2 as a protein that promotes assembly of PINK1 in a ~700-kDa complex with components of the translocon and PARK2. In the absence of HK2, there is reduced accumulation of PINK1 and PARK2 in the ~700-kDa complex and reduced levels of pS65-Ub.

labeling, and HK2$^{-/-}$ cells displayed defects in pS65-Ub accumulation 1 hour after depolarization, suggesting a role in early steps in the pathway. PINK1 formed a ~700-kDa complex, as assessed by native gel analysis (*18*), and a portion of PARK2 comigrated with this complex. However, cells lacking HK2 displayed greatly reduced levels of this PINK1-PARK2 complex, without an apparent effect on the translocon itself, because the major translocon complex at ~500 kDa as observed with α-TOMM40 was unchanged in HK2$^{-/-}$ cells (Fig. 6B). The ability of HK2 to support PINK1-PARK2 complex formation and accumulation of pS65-Ub did not require HK2 catalytic activity, its ability to be phosphorylated by AKT1, or its ubiquitylation by PARK2 on three of its major ubiquitylation sites. As such, we suggest that HK2 serves a potential scaffolding function that assists in the formation of this complex. We cannot exclude that ubiquitylation of alternative sites is required for this activity. HK2 deletion had a profound effect on mitochondrial clearance over extended time periods after depolarization. We noticed a 50% reduction in ATP levels in depolarized cells lacking HK2 at 29 hours after depolarization, when compared with WT cells (fig. S4). We cannot exclude a role for reduced ATP levels in the mitophagy defect in these cells, but ATP levels 1 hour after depolarization are not affected by loss of HK2, indicating that the defects in early steps in the pathway are unrelated to HK2's role in ATP production.

Together, these studies provide insight into the composition and requirements for formation of the mitochondrial-autophagosome synapse and provide a resource for further analysis of the mechanisms underlying PARK2-dependent mitophagy.

MATERIALS AND METHODS

Cell culture and gene editing

HFT PARK2^{WT} or the corresponding PARK2^{C431S} cells, as well as cells deficient in either PINK1, TBK1, OPTN, NDP52, or RAB7A, were generated as described previously (*9*, *44*). Cells were grown in Dulbecco's modified Eagle's medium (DMEM) with 10% fetal bovine serum (FBS) supplemented with hygromycin (200 μg/ml). PARK2 expression was induced by treating cells with doxycycline (0.5 μg/ml) as indicated. To depolarize mitochondria, cells were treated with a mixture of antimycin A (10 μM) and oligomycin A (5 μM) (Sigma) (referred to as AO) for the indicated time period. WCEs were obtained from cells washed twice with ice-cold phosphate-buffered saline (PBS) and lysed in lysis buffer [50 mM tris-HCl (pH 7.5), 150 mM NaCl, 0.5% (v/v) NP-40 (or 1% Triton X-100), and proteases/phosphatases inhibitor tablets (Roche)]. Mitochondria were purified as described previously (*44*) and subjected to lysis as indicated above.

Cas9-mediated gene editing for creation of the indicated null alleles as single-cell clones was performed by using the indicated guide sequences as described previously (*63*): TAX1BP1, CCACATCCAAAAGATTGGGT; PLA2G6, CACTGAAGGTATTGACCAGG; SEC22B, AACAATGATCGCCCGAGTGG; MFF, TGTTCCAGGTCAGCGTTTGG; IMMT, GCTGCGGGCCTGTCAGTTAT; TBC1D15, GCTGGGATGGCGAAGAGCAA; WIPI2, AATGCACACATCTTCCGTAT; MICALL1, CCTTCTGCGCCATCCTGCAC; RAB8A, GTCGGGGAGAGAGTGTAATA; TBC1D10A, GGCGGAGAGCCTGAACTCCG; TSPO, GACCCTCGCCGTGGACAAAG; HK2, CTTCCTTTCTCTGCAGAACA; HK1, GGAATGGACCTTACGAATGT. To validate gene editing, target regions were polymerase chain reaction (PCR)–amplified and sequenced, as well as validated by immunoblotting. Guide sequences used for flow cytometry–based Keima assays are as follows: GFP, GGGCGAGGAGCTGTTCACCG; TRAPPC4 #1, GGGCGGCTTGATTTACCAGT; TRAPPC4 #2, GATGTGGTGAACAAAGCTGG; RAB36 #1, GTCTTTGCAGTGGTACACGC; RAB36 #2, GCTCAAACTCTCCAAGGTGG; SYCE3 #1, GGACTCGGCCAGCGTAGGGT; SYCE3 #2, GCATGGACTCGGCCAGCGTA; TBC1D22A #1, GTTGCTCTCAAACTCCTGGA; TBC1D22A #2, GGAGAGCCTGAACTCCGAGG; WIPI2 #1, GCTGCTACTTGGCGTACCCA; WIPI2 #2, GGACTTACTACCAACAGCTA; PLA2G6 #1, GGAGGGGAGCTCTCATAGAA; PLA2G6 #2, GTGCTTCCCACCCATCCACG; ATG9A #1, GCATGTAGTTCTGGAAACGG; ATG9A #2, GTTCCTATCCCACAGCACCT; DENND6B #1, GTCCAGCAGATGCTGTCGAG; DENND6B #2, GCTGTTGTAGTGCCTGTCGT; WDR45 #1, GCCCTGTGCTCACCAGTAGA; WDR45 #2, GCAAGGCCAGAAGGTTGGAG; MICALL1 #1, GTAGGGGTGATGCCGTACCA; MICALL1 #2, GCTCCTCCTCCTCCTCAAAG; SGSM1 #1, GGTGAAGCAGATCATGGAGG; SGSM1 #2, GCTTACCCAACAAAGATGCA.

To generate HK2 point mutants, Quick Change mutagenesis was performed on the wild-type constructs by using KOD (*Thermococcus kodakaraensis*) hot polymerase (EMD Millipore) followed by Dpn I digestion. For stable expression of indicated gene, pHAGE lentiviral constructs containing the indicated open reading frames were packaged into virus, used to infect the indicated cells, and stable cell lines were selected in puromycin (1 μg/ml) as described previously.

Antibodies, immunofluorescence, and image analysis

The following antibodies were used in this study: α-MFN2 ([NIAR164], Abcam), α-TOMM20 (sc-11415, Santa Cruz Biotechnology), α-PARKIN {sc-32282, Santa Cruz Biotechnology; [EPR5024(N)], Abcam}, α-UB (sc-8017, Santa Cruz Biotechnology), α-hemagglutinin (MMS-101P, BioLegend), α-TBK1 [3013S, Cell Signaling Technology (CST)], α-p-S172 TBK1 (5483P, CST), α-actin (sc-69879, Santa Cruz Biotechnology), α-PINK1 (AW5456-U400, Abgent), α-FLAG (F1804-200UG, Sigma), α-p-S65 UB (ubiquitin) (ABS1513, EMD Millipore), α-LC3B (2775S, CST), α-GABARAP (GTX132657, GeneTex), α-CISD1 (16006-1-AP, Proteintech), α-ATG9A (ab108338, Abcam), α-ULK1 (8054S, CST), α-OPTN (ab23666, Abcam), α-FIP200 (ab227726, Abcam), α-WIPI2 (MCA5780GA, Bio-Rad), α-ATG14 (5504S, CST), α-MFF (17090-1-AP, Proteintech), α-TBC1D15 (GTX121081, GeneTex), α-NDP52 (9035S, CST), α-TOM40 (sc-365467, Santa Cruz Biotechnology), α-GABARAP (GTX132657, GeneTex), α-HK2 (2106S, CST), α-HK1 (2024S, CST), α-SEC22B (14776-1-AP, Proteintech), α-p-S6K (T389) (9206, CST), α-ATP5B (sc-55597, Santa Cruz Biotechnology), α-LC3B (3868S, CST), α-p62 (7695, CST), α-TAX1BP1 (HPA024432, Sigma), and α-UBA6 (*64*).

For immunofluorescence, cells were treated as indicated, fixed with 4% paraformaldehyde for 10 min at room temperature, washed in 1× PBS, permeabilized with ice-cold 0.2% Triton-X 100 for 3 min, washed in 1× PBS, blocked with 1% bovine serum albumin in 1× PBS, and subjected to immunostaining using indicated antibodies as previously described (*9*). Hoechst dye was used to stain the nucleus. To image cells, a Yokogawa CSU X1 spinning disk confocal lens on a Nikon Ti-E inverted microscope equipped with a 100-Å Plan Apo N.A. 1.4 objective lens in the Nikon Imaging Center at Harvard Medical School was used.

For mitophagy assays, each cell line was treated with doxycycline (0.5 μM to induce PARK2 expression) for 2.5 hours, washed, and then treated with AO as indicated. After 32 hours of AO treatment, cells were fixed, permeabilized, blocked, and immunostained with

α-DNA antibody followed by Hoechst staining as above. Images were acquired as described above. For quantification, >100 cells were counted for each replicate on the basis of the classification of unaggregated mitochondria, aggregated mitochondria, and cleared mitochondria in biological triplicate.

APEX2 proteomics/immunoblotting

To induce proximity labeling in live cells, the indicated cells were incubated with or without 500 μM biotin phenol (LS-3500.0250, Iris Biotech) for 1 hour and treated with 1 mM H_2O_2 for 1 min, and the reaction was quenched with 1× PBS supplemented with 5 mM Trolox, 10 mM sodium ascorbate, as well as 10 mM sodium azide as described previously (*60*). Cells were then harvested, and lysed in radioimmunoprecipitation assay (RIPA) buffer (supplemented with 5 mM Trolox, 10 mM sodium ascorbate, and 10 mM sodium azide). To enrich biotinylated proteins, an identical amount of cleared lysates in each cell was subjected to affinity purification by incubating with the streptavidin-coated magnetic beads (catalog no. 88817, Pierce) for 1 hour at room temperature. Beads were subsequently washed twice with RIPA buffer, once with 1 M KCl, once with 0.1 M $NaCO_3$, once with 2 M urea, twice with RIPA buffer, and three times with 1× PBS.

For immunoblotting, biotinylated proteins bound to the beads were eluted with 1× LDS (lithium dodecyl sulfate) buffer (NP0008, Invitrogen) and subjected to SDS-PAGE followed by immunoblotting with indicated antibodies.

For proteomics, biotinylated protein bound to the beads was digested with trypsin in 0.1 M EPPS [4-(2-Hydroxyethyl)-1-piperazinepropanesulfonic acid, 4-(2-Hydroxyethyl)piperazine-1-propanesulfonic acid, *N*-(2-Hydroxyethyl)piperazine-*N*′-(3-propanesulfonic acid)] (pH 8.5) overnight at 37°C. To quantify the relative abundance of individual protein across different samples, each digest was labeled with 10-plex TMT reagents (Thermo Fisher Scientific), mixed, and desalted with a C18 StageTip (packed with Empore C18; 3M Corporation) before SPS-MS^3 analysis (*42*) on an Orbitrap Fusion (Thermo Fisher Scientific) instrument as described previously (*44*). The abundance of avidin peptides was used to normalize relative protein quantity across each reporter ion channel based on the assumption that the same amount of streptavidin-coated beads was used for each sample.

Library design and preparation

We extracted all putative gRNA target sequences (based on NGG PAM sequence) from protein coding regions of all annotated human genes (GENCODE v24). These sequences were first ranked using the algorithm developed by Doench *et al.* (*65*) to narrow down to 50 gRNAs with the highest scores for each gene. We then reranked these 50 sequences based on conservation scores. Top 10 gRNA sequences were picked for each gene. Libraries of gRNAs flanked with the Bbs I (NEB) restriction site were synthesized on chip from CustomArray Inc. and Agilent. The pooled oligos were PCR-amplified, digested with Bbs I, and ligated into the Bsm BI site of the pLentiCRISPR-v2 vector (plasmid no. 52961, Addgene) for downstream applications.

The single-guide RNA (sgRNA) library was then packaged into the lentivirus, concentrated with the Lenti X-concentrator (catalog no. 631231, Takara Bio), and transduced in the HFT_$PARK2^{WT}$; mt-mKeima cell line at an MOI of 0.2 with about 500-fold representation of the library. After 7 days of selection in DMEM supplemented with 10% FBS and puromycin (1 μg/ml), cells were depolarized for the indicated time period and subjected to fluorescence-activated cell sorting from the top or bottom 10% of the entire population as described. For each sample, genomic DNA was isolated from each of the presorted and sorted cells. sgRNA sequence from each sample was PCR-amplified and subjected to Illumina next-generation sequencing for quantification followed by MAGeCK analysis to rank potential hits as previously described (*47*, *66*).

Flow cytometry

Cells stably expressing mt-mKeima were either left untreated or treated with AO for the indicated time period. Right before flow cytometry, cells were harvested, washed, and resuspended in FACS buffer [1% FBS, 1 mM EDTA, and 25 mM Hepes (pH 7) in PBS] containing DAPI (4′,6-diamidino-2-phenylindole; 5 μg/ml; Thermo Fisher Scientific) and subjected to flow cytometry (MoFlo Astrios Cell Sorter, Beckman Coulter). To determine mt-mKeima–positive cells, live single-cell population was excited at 488 and 561 nm, and their emission at 620 nm was first displayed and analyzed on BD FACSDiva software (Becton Dickinson) and subsequently analyzed by using the FlowJo software. Cell sorting and analysis were performed on either a MoFlo Astrios (Beckman Coulter) or a FACSymphony (BD Biosciences).

SDS-PAGE and immunoblotting

For SDS-PAGE, indicated cells were lysed in lysis buffer described above. Forty micrograms of whole-cell lysates (or 20 μg for purified mitochondrial lysates) was then loaded onto the SDS–polyacrylamide gel and subjected to electrophoresis. After electrophoresis, gels were transferred to polyvinylidene difluoride membrane and subjected to immunoblotting with indicated antibodies.

APEX2 EM

To prepare cells for the EM, the indicated cells were treated with AO as indicated and subjected to the workflow as reported previously (*60*). Briefly, cells were fixed using 2% glutaraldehyde (Electron Microscopy Sciences) in "buffer" [100 mM sodium cacodylate with 2 mM $CaCl_2$ (pH 7.4)] for 30 min, washed, quenched with 20 mM glycine in "buffer," and washed again. Cells were then treated with buffer containing both DAB free base (0.5 mg/ml, 1.4 mM; Sigma) and 10 mM H_2O_2 for 5 min, washed, and subjected to 2% osmium tetroxide (Electron Microscopy Sciences) staining for 30 min in ice-cold buffer followed by washing in distilled water. Cells were subsequently rinsed in maleate buffer, stained in 1% uranyl acetate in maleate buffer for 1 hour, rinsed in distilled water, and sequentially dehydrated in 70, 95, and 100% ethanol twice. The 100% ethanol was removed; 1 ml of 100% propylene oxide was added, swirled, and triturated with a polypropylene transfer pipet until the cells are lifted from the plate surface and transferred to an Eppendorf tube. The cells in tubes were centrifuged for 2 min at 15,000 rpm. The propylene oxide was pipetted off and replaced with an infiltration solution of 1:1 propylene oxide/Taab embedding resin at 4°C overnight. The samples were then brought to room temperature and centrifuged again, and the cell pellet was transferred to 100% Taab resin in an embedding mold. The residual propylene oxide was allowed to evaporate off, and the cell pellet was positioned to be cut into sections. The samples were polymerized in a 65°C oven for 48 hours and imaged with the JEOL 1200EX equipped with an Advanced Microscopy Techniques 2k charge-coupled device (CCD) camera at the Harvard Medical School Electron Microscopy Facility.

For CLEM, the indicated cells seeded on gridded coverslips (catalog no. P35G-1.5-14-CGRD, MatTek) were fixed with 2% glutaraldehyde (Electron Microscopy Sciences) in buffer as above and subjected to fluorescence microscopy by using a Yokogawa CSUX1 spinning disk confocal lens on a Nikon Ti-E inverted microscope equipped with a 100-Å Plan Apo N.A. 1.4 objective lens in the Nikon Imaging Center at Harvard Medical School. Cells were then subsequently stained with DAB and osmium tetroxide as described above. The glass coverslip was then placed in a coverslip rack and dehydrated in a graded series of ethanol using the progressive lowering of temperature method. In 100% ethanol, it was brought to room temperature, dipped in 100% propylene oxide, and infiltrated with solutions of 2:1 and 1:2 propylene oxide/Epon Araldite embedding resin before 100% resin. The coverslip was then mounted using a gasket and layers of ACLAR embedding film (product no. 10501-10, Ted Pella) and polymerized in a 65°C oven for 48 hours. The layer of ACLAR at the back of the glass coverslip was peeled away, and the glass was carefully removed using ice cubes and forceps. This resulted in a disk of embedded cells in a thin layer of resin that could then be viewed under a phase microscope to locate the specific cells and the alphanumeric imprint from the gridded glass coverslip previously imaged by phase and fluorescent microscopy. These areas of cells were then excised from the disk by razor blade and remounted on a resin dummy block for sectioning. Serial thin sections (75 nm) were cut with a DiATOME diamond knife using a Reichert Ultracut S microtome and picked up on 1 mm × 2 mm copper slot grids with Formvar support film. Immediately before viewing and imaging, the grids were contrasted with lead citrate stain. Using the phase/fluorescent overlay images as a guide, the individual cell could be identified by its "footprint" shape in the first of the serial sections collected, and APEX2/DAB-labeled organelles within those cells were identified in the series of sections of each cell. Imaging was done with a Tecnai G2 SpiritBioTWIN microscope using an AMT 2k CCD camera.

ATP content measurement

To measure the levels of cellular ATP, a luminescent ATP detection assay (ab113849, Abcam) was performed following the manufacturer's instruction.

UBA6 UB charging assay

To examine UBA6 UB charging in the cell, indicated cells were lysed in buffer containing 50 mM MES (pH 4.5), 150 mM NaCl, 0.2% Nonidet P-40, and protease inhibitors with or without 200 mM dithiothreitol as described previously (*67*).

Blue native polyacrylamide gel electrophoresis

The indicated purified mitochondrial pellet was lysed in 1× NativePAGE sample buffer (BN2003, Invitrogen) supplemented with 1% (w/v) Digitonin for 30 min on ice, and 30 μg of cleared lysates was mixed with G-250 (BN2004, Invitrogen) to a final concentration of 0.25%. Samples were then loaded on 4 to 16% bis-tris NativePAGE (BN1002BOX, Invitrogen) following the manufacturer's instructions, transferred on nitrocellulose membrane, and subjected to immunoblotting with the indicated antibodies.

Glucose 6-phosphate levels

The indicated cells were either left untreated or treated with AO for 1 hour, and 6.5 million cells from biological quintuplicate were harvested and snap-frozen in liquid nitrogen. Each cell pellet was then resuspended with ice-cold 90% methanol containing the internal standard succinic acid-2,2,3,3-d4 to give a final concentration of 80% methanol to the cell pellet. Samples were vortexed, sonicated, incubated at −20°C for 1 hour, and subsequently centrifuged at 20,000*g* for 10 min at 4°C to obtain the supernatant containing metabolites. The vacuum-dried metabolites were then subjected to gas chromatography–mass spectrometry (GC-MS) analysis by using the Agilent 7200 GC-MS QTOF and an Agilent automatic liquid sampler at the Metabolomics core facility at the University of Utah.

LysoTracker Red staining

The indicated cells were stained with 50 nM LysoTracker Red (L7528, Thermo Fisher Scientific) in DMEM media for 30 min at 37°C and washed with PBS three times. Cells were then resuspended in FACS buffer [1% FBS, 1 mM EDTA, and 25 mM Hepes (pH 7) in PBS] containing 10 μg/ml DAPI (Thermo Fisher Scientific) before analysis by flow cytometry (FACSymphony, BD Biosciences).

JC-1 staining

The indicated cells were stained with 2.5 μM JC-1 (Thermo Fisher Scientific, catalog no. T3168) for 30 min in cell culture media at 37°C. Cells were then harvested, washed, and subjected to flow cytometry (FACS-Canto) following the manufacturer's instructions. Briefly, JC-1 was excited at 488 nm and its emission at both 525 nm (FITC-A) and 585 nm (PE-A) was measured. By comparing the ratio of emission at 585 nm/525 nm, relative levels of mitochondrial membrane potential were determined from 10,000 cells in biological triplicate.

Statistical analysis

To generate bar graphs, mean and SEM were obtained from values of the indicated sample. To determine statistical significance in figs. S1 (B and C) and S3A, *P* value was obtained from two-way analysis of variance (ANOVA) with Tukey's multiple comparison test. These analyses were all performed by using the GraphPad Prism 7 software. To generate volcano plots, bar graphs, and Venn diagrams in Fig. 1 (G and H) and figs. S4 (C and D) and S2 (D and E), individual values were subjected to multiple *t* test with 1% FDR correction using GraphPad Prism 7 software.

SUPPLEMENTARY MATERIALS

Supplementary material for this article is available at http://advances.sciencemag.org/cgi/content/full/5/11/eaay4624/DC1

Fig. S1. Characterization of APEX2^{F}-OPTN recruitment to depolarized mitochondria.

Fig. S2. Analysis of proximity biotinylation using APEX2F-OPTN and APEX2^{F}-TAX1BP1 in response to mitochondrial depolarization.

Fig. S3. Benchmarking and validation of an mt-Keima–based screening platform for CRISPR-Cas9 analysis of mitophagic flux.

Fig. S4. The HK2 requirement for PINK1 activation is not due to ATP depletion and is also observed in H9 hES.

Dataset S1. Tables containing proteomic identification of proteins in proximity to APEX2-OPTN at 1 and 3 hours after depolarization determined in duplicate.

Dataset S2. Tables containing proteomic identification of proteins in proximity to APEX2-OPTN at 1 hour after depolarization in triplicate.

Dataset S3. Tables containing proteomic identification of proteins in proximity to APEX2-OPTN^{D474N} at 1 hour after depolarization in triplicate.

Dataset S4. Tables containing proteomic identification of proteins in proximity to APEX2-TAX1BP1 at 1 hour after depolarization in triplicate.

Dataset S5. Tables containing target sgRNA sequences used to create custom CRISPR libraries, as well as raw sequence reads and MAGeCK scores from the mitophagic flux screens performed using mt-Keima flux assays.

View/request a protocol for this paper from *Bio-protocol*.

REFERENCES AND NOTES

1. A. Khaminets, C. Behl, I. Dikic, Ubiquitin-dependent and independent signals in selective autophagy. *Trends Cell Biol.* **26**, 6–16 (2016).
2. P. Grumati, I. Dikic, Ubiquitin signaling and autophagy. *J. Biol. Chem.* **293**, 5404–5413 (2018).
3. N. Mizushima, T. Yoshimori, Y. Ohsumi, The role of Atg proteins in autophagosome formation. *Annu. Rev. Cell Dev. Biol.* **27**, 107–132 (2011).
4. T. N. Nguyen, B. S. Padman, J. Usher, V. Oorschot, G. Ramm, M. Lazarou, Atg8 family LC3/GABARAP proteins are crucial for autophagosome–lysosome fusion but not autophagosome formation during PINK1/Parkin mitophagy and starvation. *J. Cell Biol.* **215**, 857–874 (2016).
5. L. Pontano Vaites, J. A. Paulo, E. L. Huttlin, J. W. Harper, Systematic analysis of human cells lacking ATG8 proteins uncovers roles for GABARAPs and the CCZ1/MON1 regulator C18orf8/RMC1 in macro and selective autophagic flux. *Mol Cell Biol.* **38**, e00392–17 (2017).
6. K. Husnjak, I. Dikic, Ubiquitin-binding proteins: Decoders of ubiquitin-mediated cellular functions. *Annu. Rev. Biochem.* **81**, 291–322 (2012).
7. A. Stolz, A. Ernst, I. Dikic, Cargo recognition and trafficking in selective autophagy. *Nat. Cell Biol.* **16**, 495–501 (2014).
8. J. W. Harper, A. Ordureau, J.-M. Heo, Building and decoding ubiquitin chains for mitophagy. *Nat. Rev. Mol. Cell Biol.* **19**, 93–108 (2018).
9. J.-M. Heo, A. Ordureau, J. A. Paulo, J. Rinehart, J. W. Harper, The PINK1-PARKIN mitochondrial ubiquitylation pathway drives a program of OPTN/NDP52 recruitment and TBK1 activation to promote mitophagy. *Mol. Cell* **60**, 7–20 (2015).
10. M. Lazarou, D. A. Sliter, L. A. Kane, S. A. Sarraf, C. Wang, J. L. Burman, D. P. Sideris, A. I. Fogel, R. J. Youle, The ubiquitin kinase PINK1 recruits autophagy receptors to induce mitophagy. *Nature* **524**, 309–314 (2015).
11. E. Turco, M. Witt, C. Abert, T. Bock-Bierbaum, M. Y. Su, R. Trapannone, M. Sztacho, A. Danieli, X. Shi, G. Zaffagnini, A. Gamper, M. Schuschnig, D. Fracchiolla, D. Bernklau, J. Romanov, M. Hartl, J. H. Hurley, O. Daumke, S. Martens, FIP200 claw domain binding to p62 promotes autophagosome formation at ubiquitin condensates. *Mol. Cell* **74**, 330–346.e11 (2019).
12. J. N. S. Vargas, C. Wang, E. Bunker, L. Hao, D. Maric, G. Schiavo, F. Randow, R. J. Youle, Spatiotemporal control of ULK1 activation by NDP52 and TBK1 during selective autophagy. *Mol. Cell* **74**, 347–362.e6 (2019).
13. B. S. Padman, T. N. Nguyen, L. Uoselis, M. Skulsuppaisarn, L. K. Nguyen, M. Lazarou, LC3/GABARAPs drive ubiquitin-independent recruitment of Optineurin and NDP52 to amplify mitophagy. *Nat. Commun.* **10**, 408 (2019).
14. B. J. Ravenhill, K. B. Boyle, N. von Muhlinen, C. J. Ellison, G. R. Masson, E. G. Otten, A. Foeglein, R. Williams, F. Randow, The cargo receptor NDP52 initiates selective autophagy by recruiting the ULK complex to cytosol-invading bacteria. *Mol. Cell* **74**, 320–329.e6 (2019).
15. A. M. Pickrell, R. J. Youle, The roles of PINK1, parkin, and mitochondrial fidelity in Parkinson's disease. *Neuron* **85**, 257–273 (2015).
16. K. Yamano, N. Matsuda, K. Tanaka, The ubiquitin signal and autophagy: An orchestrated dance leading to mitochondrial degradation. *EMBO Rep.* **17**, 300–316 (2016).
17. S. Sekine, R. J. Youle, PINK1 import regulation; a fine system to convey mitochondrial stress to the cytosol. *BMC Biol.* **16**, 2 (2018).
18. M. Lazarou, S. M. Jin, L. A. Kane, R. J. Youle, Role of PINK1 binding to the TOM complex and alternate intracellular membranes in recruitment and activation of the E3 ligase Parkin. *Dev. Cell* **22**, 320–333 (2012).
19. L. A. Kane, M. Lazarou, A. I. Fogel, Y. Li, K. Yamano, S. A. Sarraf, S. Banerjee, R. J. Youle, PINK1 phosphorylates ubiquitin to activate Parkin E3 ubiquitin ligase activity. *J. Cell Biol.* **205**, 143–153 (2014).
20. A. Kazlauskaite, V. Kelly, C. Johnson, C. Baillie, C. J. Hastie, M. Peggie, T. Macartney, H. I. Woodroof, D. R. Alessi, P. G. A. Pedrioli, M. M. K. Muqit, Phosphorylation of Parkin at Serine65 is essential for activation: Elaboration of a Miro1 substrate-based assay of Parkin E3 ligase activity. *Open Biol.* **4**, 130213 (2014).
21. A. Kazlauskaite, C. Kondapalli, R. Gourlay, D. G. Campbell, M. S. Ritorto, K. Hofmann, D. R. Alessi, A. Knebel, M. Trost, M. M. K. Muqit, Parkin is activated by PINK1-dependent phosphorylation of ubiquitin at Ser65. *Biochem. J.* **460**, 127–141 (2014).
22. A. F. Schubert, C. Gladkova, E. Pardon, J. L. Wagstaff, S. M. V. Freund, J. Steyaert, S. L. Maslen, D. Komander, Structure of PINK1 in complex with its substrate ubiquitin. *Nature* **552**, 51–56 (2017).
23. C. Gladkova, S. L. Maslen, J. M. Skehel, D. Komander, Mechanism of parkin activation by PINK1. *Nature* **559**, 410–414 (2018).
24. A. Ordureau, S. A. Sarraf, D. M. Duda, J.-M. Heo, M. P. Jedrychowski, V. O. Sviderskiy, J. L. Olszewski, J. T. Koerber, T. Xie, S. A. Beausoleil, J. A. Wells, S. P. Gygi, B. A. Schulman, J. W. Harper, Quantitative proteomics reveal a feedforward mechanism for mitochondrial PARKIN translocation and ubiquitin chain synthesis. *Mol. Cell* **56**, 360–375 (2014).
25. A. Ordureau, J.-M. Heo, D. M. Duda, J. A. Paulo, J. L. Olszewski, D. Yanishevski, J. Rinehart, B. A. Schulman, J. W. Harper, Defining roles of PARKIN and ubiquitin phosphorylation by PINK1 in mitochondrial quality control using a ubiquitin replacement strategy. *Proc. Natl. Acad. Sci. U.S.A.* **112**, 6637–6642 (2015).
26. K. Shiba-Fukushima, Y. Imai, S. Yoshida, Y. Ishihama, T. Kanao, S. Sato, N. Hattori, PINK1-mediated phosphorylation of the Parkin ubiquitin-like domain primes mitochondrial translocation of Parkin and regulates mitophagy. *Sci. Rep.* **2**, 1002 (2012).
27. A. Kazlauskaite, R. J. Martínez-Torres, S. Wilkie, A. Kumar, J. Peltier, A. Gonzalez, C. Johnson, J. Zhang, A. G. Hope, M. Peggie, M. Trost, D. M. F. van Aalten, D. R. Alessi, A. R. Prescott, A. Knebel, H. Walden, M. M. K. Muqit, Binding to serine 65-phosphorylated ubiquitin primes Parkin for optimal PINK1-dependent phosphorylation and activation. *EMBO Rep.* **16**, 939–954 (2015).
28. T. Wauer, M. Simicek, A. Schubert, D. Komander, Mechanism of phospho-ubiquitin-induced PARKIN activation. *Nature* **524**, 370–374 (2015).
29. S. Geisler, K. M. Holmström, D. Skujat, F. C. Fiesel, O. C. Rothfuss, P. J. Kahle, W. Springer, PINK1/Parkin-mediated mitophagy is dependent on VDAC1 and p62/SQSTM1. *Nat. Cell Biol.* **12**, 119–131 (2010).
30. N. C. Chan, A. M. Salazar, A. H. Pham, M. J. Sweredoski, N. J. Kolawa, R. L. J. Graham, S. Hess, D. C. Chan, Broad activation of the ubiquitin-proteasome system by Parkin is critical for mitophagy. *Hum. Mol. Genet.* **20**, 1726–1737 (2011).
31. S. A. Sarraf, M. Raman, V. Guarani-Pereira, M. E. Sowa, E. L. Huttlin, S. P. Gygi, J. W. Harper, Landscape of the PARKIN-dependent ubiquitylome in response to mitochondrial depolarization. *Nature* **496**, 372–376 (2013).
32. C. M. Rose, M. Isasa, A. Ordureau, M. A. Prado, S. A. Beausoleil, M. P. Jedrychowski, D. J. Finley, J. W. Harper, S. P. Gygi, Highly multiplexed quantitative mass spectrometry analysis of ubiquitylomes. *Cell Syst.* **3**, 395–403.e4 (2016).
33. A. Ordureau, J. A. Paulo, W. Zhang, T. Ahfeldt, J. Zhang, E. F. Cohn, Z. Hou, J. M. Heo, L. L. Rubin, S. S. Sidhu, S. P. Gygi, J. W. Harper, Dynamics of PARKIN-dependent mitochondrial ubiquitylation in induced neurons and model systems revealed by digital snapshot proteomics. *Mol. Cell* **70**, 211–227.e8 (2018).
34. Y. C. Wong, E. L. Holzbaur, Optineurin is an autophagy receptor for damaged mitochondria in parkin-mediated mitophagy that is disrupted by an ALS-linked mutation. *Proc. Natl. Acad. Sci. U.S.A.* **111**, E4439–E4448 (2014).
35. A. S. Moore, E. L. Holzbaur, Dynamic recruitment and activation of ALS-associated TBK1 with its target optineurin are required for efficient mitophagy. *Proc. Natl. Acad. Sci. U.S.A.* **113**, E3349–E3358 (2016).
36. B. Richter, D. A. Sliter, L. Herhaus, A. Stolz, C. Wang, P. Beli, G. Zaffagnini, P. Wild, S. Martens, S. A. Wagner, R. J. Youle, I. Dikic, Phosphorylation of OPTN by TBK1 enhances its binding to Ub chains and promotes selective autophagy of damaged mitochondria. *Proc. Natl. Acad. Sci. U.S.A.* **113**, 4039–4044 (2016).
37. G. Beutner, A. Ruck, B. Riede, D. Brdiczka, Complexes between hexokinase, mitochondrial porin and adenylate translocator in brain: Regulation of hexokinase, oxidative phosphorylation and permeability transition pore. *Biochem. Soc. Trans.* **25**, 151–157 (1997).
38. V. Hung, S. S. Lam, N. D. Udeshi, T. Svinkina, G. Guzman, V. K. Mootha, S. A. Carr, A. Y. Ting, Proteomic mapping of cytosol-facing outer mitochondrial and ER membranes in living human cells by proximity biotinylation. *eLife* **6**, e24463 (2017).
39. C. E. Gleason, A. Ordureau, R. Gourlay, J. S. Arthur, P. Cohen, Polyubiquitin binding to optineurin is required for optimal activation of TANK-binding kinase 1 and production of interferon β. *J. Biol. Chem.* **286**, 35663–35674 (2011).
40. F. Li, D. Xu, Y. Wang, Z. Zhou, J. Liu, S. Hu, Y. Gong, J. Yuan, L. Pan, Structural insights into the ubiquitin recognition by OPTN (optineurin) and its regulation by TBK1-mediated phosphorylation. *Autophagy* **14**, 66–79 (2018).
41. D. Narendra, L. A. Kane, D. N. Hauser, I. M. Fearnley, R. J. Youle, p62/SQSTM1 is required for Parkin-induced mitochondrial clustering but not mitophagy; VDAC1 is dispensable for both. *Autophagy* **6**, 1090–1106 (2014).
42. G. C. McAlister, D. P. Nusinow, M. P. Jedrychowski, M. Wühr, E. L. Huttlin, B. K. Erickson, R. Rad, W. Haas, S. P. Gygi, MultiNotch MS3 enables accurate, sensitive, and multiplexed detection of differential expression across cancer cell line proteomes. *Anal. Chem.* **86**, 7150–7158 (2014).
43. K. Yamano, C. Wang, S. A. Sarraf, C. Münch, R. Kikuchi, N. N. Noda, Y. Hizukuri, M. T. Kanemaki, W. Harper, K. Tanaka, N. Matsuda, R. J. Youle, Endosomal Rab cycles regulate Parkin-mediated mitophagy. *eLife* **7**, e31326 (2018).
44. J.-M. Heo, A. Ordureau, S. Swarup, J. A. Paulo, K. Shen, D. M. Sabatini, J. W. Harper, RAB7A phosphorylation by TBK1 promotes mitophagy via the PINK-PARKIN pathway. *Sci. Adv.* **4**, eaav0443 (2018).
45. N. Sun, D. Malide, J. Liu, I. I. Rovira, C. A. Combs, T. Finkel, A fluorescence-based imaging method to measure in vitro and in vivo mitophagy using mt-Keima. *Nat. Protoc.* **12**, 1576–1587 (2017).
46. H. Katayama, T. Kogure, N. Mizushima, T. Yoshimori, A. Miyawaki, A sensitive and quantitative technique for detecting autophagic events based on lysosomal delivery. *Chem. Biol.* **18**, 1042–1052 (2011).
47. W. Li, J. Köster, H. Xu, C. H. Chen, T. Xiao, J. S. Liu, M. Brown, X. S. Liu, Quality control, modeling, and visualization of CRISPR screens with MAGeCK-VISPR. *Genome Biol.* **16**, 281 (2015).

48. D. G. McEwan, D. Popovic, A. Gubas, S. Terawaki, H. Suzuki, D. Stadel, F. P. Coxon, D. Miranda de Stegmann, S. Bhogaraju, K. Maddi, A. Kirchof, E. Gatti, M. H. Helfrich, S. Wakatsuki, C. Behrends, P. Pierre, I. Dikic, PLEKHM1 regulates autophagosome-lysosome fusion through HOPS complex and LC3/GABARAP proteins. *Mol. Cell* **57**, 39–54 (2015).
49. C. A. Lamb, S. Nühlen, D. Judith, D. Frith, A. P. Snijders, C. Behrends, S. A. Tooze, TBC1D14 regulates autophagy via the TRAPP complex and ATG9 traffic. *EMBO J.* **35**, 281–301 (2016).
50. F. Nishiumi, M. Ogawa, Y. Nakura, Y. Hamada, M. Nakayama, J. Mitobe, A. Hiraide, N. Sakai, M. Takeuchi, T. Yoshimori, I. Yanagihara, Intracellular fate of Ureaplasma parvum entrapped by host cellular autophagy. *Microbiologyopen* **6**, e00441 (2017).
51. K. Shirahama-Noda, S. Kira, T. Yoshimori, T. Noda, TRAPPIII is responsible for vesicular transport from early endosomes to Golgi, facilitating Atg9 cycling in autophagy. *J. Cell Sci.* **126**, 4963–4973 (2013).
52. D. Stanga, Q. Zhao, M. P. Milev, D. Saint-Dic, C. Jimenez-Mallebrera, M. Sacher, TRAPPC11 functions in autophagy by recruiting ATG2B-WIPI4/WDR45 to preautophagosomal membranes. *Traffic* **20**, 325–345 (2019).
53. E. Y. Chan, S. Kir, S. A. Tooze, siRNA screening of the kinome identifies ULK1 as a multidomain modulator of autophagy. *J. Biol. Chem.* **282**, 25464–25474 (2007).
54. N. Hosokawa, T. Hara, T. Kaizuka, C. Kishi, A. Takamura, Y. Miura, S. I. Iemura, T. Natsume, K. Takehana, N. Yamada, J. L. Guan, N. Oshiro, N. Mizushima, Nutrient-dependent mTORC1 association with the ULK1-Atg13-FIP200 complex required for autophagy. *Mol. Biol. Cell* **20**, 1981–1991 (2009).
55. S. A. Hasson, L. A. Kane, K. Yamano, C. H. Huang, D. A. Sliter, E. Buehler, C. Wang, S. M. Heman-Ackah, T. Hessa, R. Guha, S. E. Martin, R. J. Youle, High-content genome-wide RNAi screens identify regulators of parkin upstream of mitophagy. *Nature* **504**, 291–295 (2013).
56. A. K. Corona, W. T. Jackson, Finding the middle ground for autophagic fusion requirements. *Trends Cell Biol.* **28**, 869–881 (2018).
57. C. J. Shoemaker, T. Q. Huang, N. R. Weir, N. J. Polyakov, S. W. Schultz, V. Denic, CRISPR screening using an expanded toolkit of autophagy reporters identifies TMEM41B as a novel autophagy factor. *PLOS Biol.* **17**, e2007044 (2019).
58. K. Morita, Y. Hama, T. Izume, N. Tamura, T. Ueno, Y. Yamashita, Y. Sakamaki, K. Mimura, H. Morishita, W. Shihoya, O. Nureki, H. Mano, N. Mizushima, Genome-wide CRISPR screen identifiesTMEM41Bas a gene required for autophagosome formation. *J. Cell Biol.* **217**, 3817–3828 (2018).
59. M. K. McCoy, A. Kaganovich, I. N. Rudenko, J. Ding, M. R. Cookson, Hexokinase activity is required for recruitment of parkin to depolarized mitochondria. *Hum. Mol. Genet.* **23**, 145–156 (2014).
60. S. S. Lam, J. D. Martell, K. J. Kamer, T. J. Deerinck, M. H. Ellisman, V. K. Mootha, A. Y. Ting, Directed evolution of APEX2 for electron microscopy and proximity labeling. *Nat. Methods* **12**, 51–54 (2015).
61. P. Wild, H. Farhan, D. G. McEwan, S. Wagner, V. V. Rogov, N. R. Brady, B. Richter, J. Korac, O. Waidmann, C. Choudhary, V. Dotsch, D. Bumann, I. Dikic, Phosphorylation of the autophagy receptor optineurin restricts Salmonella growth. *Science* **333**, 228–233 (2011).
62. B. Bingol, J. S. Tea, L. Phu, M. Reichelt, C. E. Bakalarski, Q. Song, O. Foreman, D. S. Kirkpatrick, M. Sheng, The mitochondrial deubiquitinase USP30 opposes parkin-mediated mitophagy. *Nature* **510**, 370–375 (2014).
63. F. A. Ran, P. D. Hsu, J. Wright, V. Agarwala, D. A. Scott, F. Zhang, Genome engineering using the CRISPR-Cas9 system. *Nat. Protoc.* **8**, 2281–2308 (2013).
64. P. C. Lee, M. E. Sowa, S. P. Gygi, J. W. Harper, Alternative ubiquitin activation/conjugation cascades interact with N-end rule ubiquitin ligases to control degradation of RGS proteins. *Mol. Cell* **43**, 392–405 (2011).
65. J. G. Doench, N. Fusi, M. Sullender, M. Hegde, E. W. Vaimberg, K. F. Donovan, I. Smith, Z. Tothova, C. Wilen, R. Orchard, H. W. Virgin, J. Listgarten, D. E. Root, Optimized sgRNA design to maximize activity and minimize off-target effects of CRISPR-Cas9. *Nat. Biotechnol.* **34**, 184–191 (2016).
66. I. Koren, T. Timms, T. Kula, Q. Xu, M. Z. Li, S. J. Elledge, The eukaryotic proteome is shaped by E3 ubiquitin ligases targeting C-terminal degrons. *Cell* **173**, 1622–1635.e14 (2018).
67. J. Jin, X. Li, S. P. Gygi, J. W. Harper, Dual E1 activation systems for ubiquitin differentially regulate E2 enzyme charging. *Nature* **447**, 1135–1138 (2007).

Acknowledgments: We acknowledge the Nikon Imaging Center at Harvard Medical School for assistance with light microscopy. **Funding:** This work was supported by the NIH (R37 NS083524 and RO1 GM095567 to J.W.H. and K01DK098285 to J.A.P.), the Michael J. Fox Foundation (no. 15866 to J.W.H.), a Sara Elizabeth O'Brien Trust Postdoctoral Fellowship (J.-M.H.), and a gift from N. Goodnow (J.W.H.). Metabolomics analysis performed at the University of Utah was supported by NIH grants OD016232-01, OD021505-01, and DK110858-01. **Author contributions:** J.-M.H. and J.W.H. conceived the study. J.-M.H. created cell lines; performed proteomics, genetic screens, autophagy, and trafficking CRISPR library construction; and performed all biochemical and cell biological experiments. N.J.H. created and characterized cell lines and performed proteomics experiments. J.A.P. performed mass spectrometry. S.J.E., M.L., and Q.X. created and provided CRISPR libraries. M.C. performed CLEM experiments. J.W.H. and J.-M.H. wrote the paper with input from all authors. **Competing interests:** J.W.H. is a founder and advisory board member for Caraway Therapeutics Inc. and a consultant for X-Chem Inc. S.J.E. is an Investigator with the Howard Hughes Medical Institute. **Data and materials availability:** All data needed to evaluate the conclusions in the paper are present in the paper and/or the Supplementary Materials. Additional data related to this paper may be requested from the authors.

Submitted 25 June 2019
Accepted 16 September 2019
Published 6 November 2019
10.1126/sciadv.aay4624

Citation: J.-M. Heo, N. J. Harper, J. A. Paulo, M. Li, Q. Xu, M. Coughlin, S. J. Elledge, J. W. Harper, Integrated proteogenetic analysis reveals the landscape of a mitochondrial-autophagosome synapse during PARK2-dependent mitophagy. *Sci. Adv.* **5**, eaay4624 (2019).